Algal Research
December 2016, Volume 20 Pages 229-248
http://dx.doi.org/10.1016/j.algal.2016.10.017
http://archimer.ifremer.fr/doc/00356/46702/

Use of a lipid rich strain reveals mechanisms of nitrogen limitation and carbon partitioning in the haptophyte *Tisochrysis lutea*

Garnier Matthieu [1, *], Bougaran Gael [1], Pavlovic Marija [2], Berard Jean-Baptiste [1], Carrier Gregory [1], Charrier Aurelie [1], Le Grand Fabienne [3], Lukomska Ewa [1], Rouxel Catherine [1], Schreiber Nathalie [1], Cadoret Jean-Paul [1], Rogniaux Hélène [2], Saint-Jean Bruno [1]

[1] IFREMER, PBA, Rue de l'Ile d'Yeu, BP 21105, 44311 Nantes Cedex 03, France
[2] INRA UR1268 BIA, rue de la Géraudière, BP71627, 44313 Nantes Cedex 03, France
[3] CNRS, Univ Brest, IRD, Ifremer, LEMAR, IUEM, Place Nicolas Copernic, 29280 Plouzané, France

* Corresponding author : Matthieu Garnier, email addresses : matthieu.garnier@ifremer.fr ; mgarnier@ifremer.fr

Abstract :

Haptophytes are a diverse monophyletic group with a worldwide distribution, known to be significantly involved in global climate regulation in their role as a carbon sink. Because nitrogen is a major limiting macronutrient for phytoplankton in oceans and for cultures of microalgae, understanding the involvement of nitrogen availability in haptophyte carbon partitioning is of global and biotechnological importance. Here, we made an ecophysiological study coupled with comprehensive large scale proteomic analysis to examine differences of behavior in reaction to nitrogen availability changes between a wild type strain of *Tisochrysis lutea* (WTc1) and a mutant strain (2Xc1) known to accumulate more storage lipids. Strains were grown in chemostats and studied under different ecophysiological conditions including N limitation, N repletion and N depletion. Whereas short time N repletion triggered consumption of carbohydrates in both strains, storage lipid degradation and accumulation during changes of ecophysiological status were recorded in 2Xc1 but not in WTc1. After 3 months of continuous culture, 2Xc1 exhibited an unexpected increase of carbon sequestration ability (+ 50%) by producing twofold more carbohydrates for the same nitrogen availability. Deep proteomic analysis by LC-MS/MS identified and compared the abundance of 4332 proteins, i.e. the deepest coverage of a microalgal proteome obtained to date. Results revealed that storage lipid accumulation is favored by an overall reorganization of carbon partitioning in 2Xc1 cells that increases the metabolism of carbon and energy acquisition, and decreases mitochondrial activity and metabolic conversion of storage lipids to phosphoenolpyruvate before gluconeogenesis.

Graphical abstract :

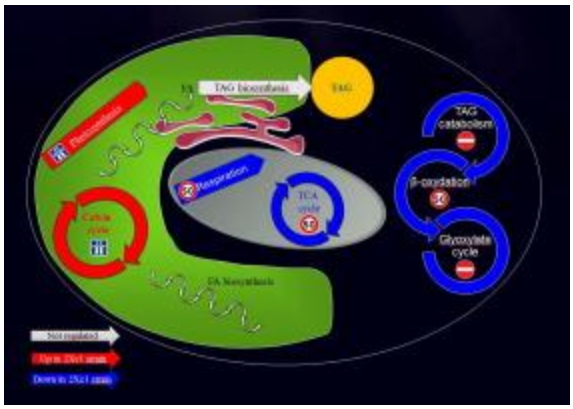

Highlights

► The high lipid strain 2Xc1 is more sensitive to changes of nitrogen availability. ► 2Xc1 is a plastic strain that increased its ability to acquire carbon. ► Carbohydrates productivity was 2-fold increase after 3 months in chemostat. ► Deep proteomics revealed a novel in-cell carbon partitioning. ► Ca^{2+}/calmodulin protein kinases may participate to the 2Xc1 behavior.

Keywords : Algae, *Isochrysis*, Lipids, Nitrogen, Reverse genomic: proteomic

1. Introduction

Photosynthetic eukaryotes make a significant contribution to major global processes, such as oxygen production, carbon fixation and CO_2 sequestration and nutrient recycling, thereby sustaining the life of most other aquatic organisms. Because of their photo-autotrophic abilities, microalgae behave as sunlight-driven cellular factories that convert CO_2 into energy-rich storage compounds such as polymeric carbohydrates and lipids [1].Hence they have received a considerable amount of attention as possible sources of next-generation energy feedstock, animal feeds, food and high valuable compounds [2,3]. The sequestration of atmospheric CO_2 by microalgae and their in-cell carbon partitioning is relevant both on a global level and to biotechnological innovation [4]. In oceans, nitrogen is the main nutrient likely to limit growth of phytoplankton [5,6]. Moreover, nitrogen availability is one of the main drivers of carbon storage and partitioning in microalgae. The overall metabolism and molecular mechanisms of storage lipid accumulation following nitrogen deprivation have been documented in detail in the model green alga *Chlamydomonas reinhardtii g*rown mixotrophically using CO_2 and acetate as carbon sources [7–13]. Other studies deal with autotrophically grown microalgae and concern *C. reinhardtii* [14], as well as diatoms of ecological interest, such as *Phaeodactylum tricornutum* [15–18] , and species used in biotechnological applications, such as the EUSTIGMATOPYCEAE *Nannochloropsis oceanica* [19,20]. A general finding of these functional genomics studies has been that lipid accumulation is connected to changes in the expression of the core enzymes of the central carbon metabolism [21]. Remarkably, changes in the enzymes of lipid metabolism are rarely observed during TAG accumulation [8,12,18,19], indicating the existence of other control points for the process of lipid accumulation. Species and physiological specificity (mixotrophy *vs* autotrophy; short term N deprivation *vs* long term deprivation) were revealed

but regulatory mechanisms remain poorly understood. Experimental approaches using mutant and complemented strains have enabled an assessment of the role of genes in lipid metabolism and deciphered carbon partitioning between carbohydrates and lipids in several species including *Chlorella sorokiniana*, *C. reinhardtii* and *P. tricornutum* [22–29]. However, although knowledge on the metabolic pathways of model species *C. reinhardtii* and *P. tricornutum* has improved, numerous papers attest that metabolic pathways and carbon storage can differ a great deal between different lineages of algae [30–32].

The haptophyte *Tisochrysis lutea* is a mobile non-calcified species that produces a high amount of docosahexanoic acid (DHA) and storage lipids, of interest for nutritional and energy applications, respectively [33,34]. T. *lutea* is widely used to feed mollusk larvae in aquaculture. It produces alkenones, which are long-chain unsaturated methyl and ethyl n-ketones (C37 and C38), exclusive to haptophytes, and widely used as biomarkers for the reconstruction of marine paleoclimatology [35-37]. Haptophytes constitute a diverse monophyletic group that originated from secondary endosymbiosis of a red alga into a non-photosynthetic eukaryotic host. The group includes calcified and non-calcified morphotypes depending on sex and species. Haptophytes are distributed worldwide and participate greatly in global climate regulation as a carbon sink [37]. For these reasons, Haptophytes are used as a biological model for studies on microalgal ecophysiology, lipid metabolism, nutrition, and toxicology [38–42]. Understanding mechanisms of carbon partitioning in haptophytes is also of ecological and biotechnological relevance. Carbon partitioning and flows toward macromolecules have been described in the blooming coccolitophoride *Emiliania huxleyi* [38,39]. The impact of nitrogen and phosphorus availability on carbon accumulation and partitioning was modeled in *T. lutea* [43–45]. However, very little is known about the metabolic pathways and regulations of carbon partitioning in *T. lutea*.

A lipid over-accumulating mutant strain (*T. lutea* S2M2) was obtained through a domestication process [46]. Forward genomics on lipid accumulating strains by comparative genomics would identify the potential metabolic controller that promotes carbon accumulation. Previous proteomic and transcriptomic analysis reveals that wild type and mutant strains behave differently during the early phases of nitrogen starvation and suggest that proteins involved in carbon homeostasis, lipid metabolism and carbohydrate catabolism are likely involved in lipid accumulation [47,48]. These studies focused on the effect of nitrogen starvation, but very little is yet known about nitrogen limitation or short-term nitrogen repletion. The objective of the current study was to characterize the ability of *T. lutea* WT and S2M2 to accumulate carbon or consume stored carbon following fine-tuned changes of nitrogen availability and to identify the molecular mechanisms involved in strain-specific metabolism. To compare strain with similar genetic diversity, this study was done with clones isolated from each strain (WTc1 from WT and 2Xc1 from S2M2). They were grown for 3 months in chemostats with nitrogen limitation and subjected to three nitrogen spikes. On the basis of growth limitation and lipid accumulation models [44,49], our hypothesis was that each nitrogen spike would lead to three successive physiological states including: 1) state of nitrogen limitation at the steady state phase before N spike and leading to storage lipid accumulation, 2) state of nitrogen repletion after N spike and leading to storage lipid consumption, and 3) state of nitrogen depletion when all the nitrogen is consumed and leading to storage lipid accumulation. The physiology, carbohydrates and lipid profiles of the two strains were studied during the experiment.

In microalgae, proteomics have provided research contributions in the areas of cell biology [50–53], metabolism [17,54–56], stress and signaling [57–60], evolution [61–63] and biotechnology [26,54,64–67]. Two-dimensional gel electrophoresis (2-DE) followed by protein identification by mass spectrometry is the main technique for comparative analysis in

138 microalgae, but label free analysis are increasingly being used, notably for the study of
139 phosphorus and nitrogen availability [8,68–71]. Last published works let to analyze the
140 abundance of 3175 proteins in *P. tricornutum* [72], 3923 proteins in *C. reinhardtii* [71]*, and*
141 2836 proteins in *Picochlorum sp*. [70]. These results encourage the use of free label
142 proteomics for the study of haptophytes. The deep whole cell proteomic analysis of
143 haptophyte has never been performed but a recent published work let to identify 514 proteins
144 from isolated lipid bodies of *T. lutea* [73]. In one of our last publication, we used 2-DE to
145 study the effect of nitrogen starvation in wild type and mutant strain of *T. lutea* and our results
146 suggested that proteomic changes may be related to carbon partitioning in S2M2 [47].

147 In the present study, a large-scale label free quantitative proteomics approach was used to
148 identify the proteins differentially accumulated in the mutant strain of *T. lutea* subjected to the
149 aforementioned conditions of nitrogen supply. The data collected offer the most
150 comprehensive view of the proteome of a microalga obtained to date, and provide new
151 mechanistic insights into lipid accumulation and carbon partitioning in haptophytes.

152

153

154

155

156

2. Results

2.1 Physiology in chemostat cultures

WTc1 and 2Xc1 strains were cultured for 90 days in nitrogen-limited chemostats, which were subjected to three nitrogen spikes. Cell Concentration (CC), Particulate Carbon (PC), Particulate Nitrogen (PN), particulate N/C ratio, Dissolved Inorganic Nitrogen (DIN) and Dissolved Inorganic Phosphorus (DIP) were sampled at high frequency throughout the course of the experiment (Fig. 1). Three phases of steady state (SS) were delimited, each of which had calculated coefficients of variation (CVs) less than 5% for PN, PC and N/C. This confirmed the low variability of algal physiology within each SS and the appropriateness of using samples taken during these phases to obtain high-quality reproducible data. CC was lower in 2Xc1 than WTc1 throughout the experiment for similar PN concentrations and similar or higher PC concentration in 2Xc1 (Fig. 1). Romanova *et. al* (2010) [74] assume that for similar amount of organic matter, a difference of cell concentration results from a difference of cell size. Therefore, our results suggest that 2Xc1 cells are bigger than the WTc1 cells.

During the dynamic phase after N spikes, CC, DIP, DIN, PC, PN and N/C ratio showed similar profiles both between the strains and for the three spikes (Fig. 1). DIN decreased quickly from 200 µM to a non-detectable concentration (< 0.5µM) in 24 hours, which was correlated with an increase of 200 µM in PN and a 30 to 35% increase of N/C ratio. This indicates a rapid N uptake by strains whose growth is limited by nitrogen. After each spike, biomass estimated by PC and CC increased drastically during the first 24 hours, demonstrating the limitation by nitrogen during SS. Then, CC and PC maintained a high level for 36 hours and decreased slightly until a new steady state was reached within 10 days.

180 Following N/C evolution, three physiological states were observed: nitrogen limitation at
181 steady state; nitrogen repletion during about 24 H, when N/C ratio increased; and nitrogen
182 depletion, when N/C ratio decreased (Fig. 1).

183 Computed growth rate was 0.5 d^{-1} at steady state and increased for 48 hours up to 0.75 d^{-1}
184 after each N spike, then decreased over 48 hours to a minimum of 0.4 d^{-1} and reached steady
185 state within 10 days (Supp mat 1).

186 ## 2.2 Carbon partitioning

187 Carbon partitioning between storage lipids, membrane lipids, carbohydrates, proteins and
188 chlorophyll for the three nitrogen physiological states has been studied on the basis of
189 conversion factors of gram carbon by gram of compound proposed by [75] (Tab. 1). Up to
190 10.7% and 27.5% of the carbon were not recorded in WTc1 and 2Xc1 respectively. This may
191 partially due to bias in the conversion factor and the absence of measurement of other organic
192 carbon compounds such as small metabolites and/or mineral carbon. As was generally found
193 in this experiment, carbon was mainly allocated to proteins, carbohydrates and membrane
194 lipids, and at a lower level to storage lipids. Throughout the experiment, proteins were 1.4 to
195 1.9-fold higher in WTc1 than in 2Xc1, chlorophyll was 1.2 to 1.8-fold higher in WTc1 and
196 storage lipids were more than twofold higher in 2Xc1 (0.6 to 3.9% of carbon in WTc1 and 3.7
197 to 9.3% in 2Xc1). Membrane lipid (ML) content was quite similar in the two strains.

198 Principal Component Analysis of the different variables of the Tab. 1 indicated that the N/C
199 ratio was correlated with the allocation of carbon to chlorophyll a and protein and inversely
200 correlated with carbohydrates in the first dimension of the PCA (70% of the observed
201 variability) (Supp mat 2). The storage lipids (SL) at steady states were mainly composed of
202 triacylglycerols (TAG) (72 to 85 % of SL in WTc1 and 95-98 % in 2Xc1) (Supp mat 3). In
203 WTc1, 9 to 28 % of the storage lipids were alkenones, whereas alkenones were very low

(<2% of SL) in 2Xc1. After the N spikes, cell storage lipid content, followed by Nile Red (NR) fluorescence and High Performance Thin Layer Chromatography (HPTLC), decreased in 2Xc1 during all phases of nitrogen repletion and increased during nitrogen depletion (Fig. 2). HPTLC analysis after the first and the second N spikes showed that membrane and storage lipids of 2Xc1 cells evolve in opposite directions suggesting that a transfer of fatty acids could occur from membrane to lipid droplets colored with Nile red. In absence of membrane lipid analysis during the third N replete state, this conclusion should be taken with caution. Lipid content in WT cells did not change after an N spike. Our results indicate that 2Xc1 accumulates more storage lipids than WT strain as previously reported [46] and is more sensitive to changes in nitrogen limitation.

During the dynamic phase after N spikes, carbohydrate content (CH) decreased drastically in cells of both strains during nitrogen repletion, then increased during nitrogen depletion (Fig. 2). Carbohydrate content was similar in the two strains at SS1, but a 100% increase was observed from SS1 to SS3 in 2Xc1 (Fig. 2). As a result, carbohydrate content in 2Xc1 was twofold higher in 2Xc1 at SS3. Moreover, for the same PN a 50% increase of PC was measured in 2Xc1 from the first SS to the third SS (+20% from SS1 to SS2; + 22% from SS2 to SS3) related to a decrease of N/C ratio (Fig. 1). This suggests an increase of carbon accumulation capacity of the 2Xc1 strain during the experiment due to an increase of cell carbohydrate content.

2.3 First comprehensive proteome analysis of *Tisochrysis lutea* reveals large differences between mutant and wild type strains

Proteomes were analyzed on samples taken during the steady states of the chemostats. Three biological samples (Pt27, Pt74 and Pt117 on Fig. 2) were used for each of the three steady

states. A large-scale proteomics analysis of the two strains and three replicates led to the identification of 4,332 proteins clustered in 4,137 groups by testing 45,032 unique peptides matching on the *T. lutea* database. The coverage of proteins by unique peptides ranged from 2 to 96 peptides per protein, with a median of 6 peptides per protein (Supp mat 4).The identified proteome represents 25% of the *in silico* predicted proteome. Yet, the function of 2,177 proteins remains unknown due to the lack of BLAST results from the Uniprot database and absence of clear functional domain annotation. Of these unknown proteins, 1,530 have homologies with proteins of unknown function in other microalgae, including 1,415 with the haptophyte *E. huxleyi*, 427 with the diatom *P. tricornutum* and 301 with the chlorophycea *C. reinhardtii*. This reveals the lack of functional knowledge on proteins of *T. lutea* although their study may have significance for the study of haptophyte and model species metabolism. The 2,155 proteins whose putative function has been inferred represent all functional categories of the cell. The most represented categories are central metabolism & energy and transcription & translation, with 410 and 359 identified proteins, respectively. Of the 254 unique EC numbers (Enzyme Commission numbers) identified, 206 were classified as belonging to major metabolic pathways. Almost all of the essential reactions involved in the major energetic and metabolic pathways were identified in this proteome: Calvin cycle, glycolysis, gluconeogenesis, tricarboxylic acid (TCA) cycle, glyoxylate cycle, and pentose phosphate pathway (Fig. 3C). The high protein coverage (median = 6 peptides per protein), the comprehensiveness of the identified proteome (4,332 proteins), and the identification of key enzymes underlines the quality of the data, meaning we can have confidence in the subsequent exploitation of these data for quantitative comparison of the protein expression profiles between the two strains.

Results of peptide normalization, protein quantification and functional annotation are available as supplementary data (Supp mat 5). Principal component analysis on the whole

253 proteome clearly showed two distinct clusters corresponding to the two strains, with 45.4% of
254 the differences observed on the first dimension and 26.5% on the second (Fig. 3A). This
255 shows strain specificities of the proteomes and justifies comparative analysis. In terms of
256 abundance, 19% of the proteins therefore differed between the strains, with 205 up-
257 accumulated and 608 down-accumulated proteins in 2Xc1, as visualized on the vulcanoplot in
258 Fig. 3B. The function of 66% of the up-accumulated proteins and 48% of the down-
259 accumulated proteins remains unknown. Yet, the results of the present paper indicate that
260 proteins whose functional annotation could be retrieved and whose abundance is altered
261 between strains are involved in numerous functional categories. The results of functional
262 classification, fold changes and *p* values are reported in Tab. 2 for up-accumulated proteins
263 and Tab. 3 for down-accumulated proteins.

264 Observed differences in the proteome profile between WT and 2Xc1 strains are discussed
265 below, according to the functional category of the proteins.

266 2.4 2Xc1 strain increases its carbon accumulation

267 Four proteins of the Calvin cycle were up-accumulated in 2Xc1, including GAPDH(NADP+),
268 PPK, and two of the three identified FBPA (Tab. 2). Two components of photosystem II
269 (PsbP and PsbU) were up-accumulated as well as three components of the photosynthetic
270 electron transport (cyc6 and FNR1), indicating increased cyclic phosphorylation (Tab. 2).
271 Conversely, two components of the photosystem I (PsaA and PsaB) were down-accumulated
272 (Tab. 3), while components of cytochrome B6F complex were not differentially accumulated.
273 Altogether, these results suggest an increase of the protein pool involved in carbon acquisition
274 mechanisms (Fig. 4).

275 2.5 Mitochondrial machinery differs strongly between strains

276 The multi-enzyme complex pyruvate dehydrogenase (PDH) converts pyruvate into acetyl-
277 CoA. It consists of three main enzymes: pyruvate dehydrogenase (PDC-E1) composed of 2
278 subunits (α and β), dihydrolipoamide S-acetyltransferase (PDC-E2), and dihydrolipoyl
279 dehydrogenase (PDC-E3). All components and two isoforms for E1 and E2 were identified in
280 *T. lutea* proteome including the chloroplastic and mitochondrial isoforms. The mitochondrial
281 isoform of PDC-E2 was 2.7-fold down-accumulated in 2Xc1 (Tab. 3). Moreover, the
282 mitochondrial pyruvate dehydrogenase kinase (PDHK), an inhibitor of PDH, was 3.8-fold up-
283 accumulated (Tab. 2). In photoautotrophic cells, the PDH pathway can be shunted by the
284 decarboxylation of pyruvate by pyruvate decarboxylase followed by the decarboxylation of
285 acetaldehyde by Acetaldehyde dehydrogenase (ALDH) and the conversion of acetate to
286 acetyl-CoA by Acetyl-coenzyme A synthetase (ACS). ALDH and ACS were both strongly
287 down-accumulated in 2Xc1 (Tab. 3). We thus conclude there was a decrease of pyruvate-
288 related hub enzymes and acetyl-CoA synthesis in mitochondria in 2Xc1 (Fig. 4).

289 Acetyl-CoA is the main entry of the TCA cycle and can be shunted by pyruvate carboxylase
290 (PCr) that converts pyruvate into oxaloacetate. PCr was also 2.8-fold down-accumulated in
291 2Xc1 (Tab. 2). Proteins involved in the first three successive reactions of the TCA cycle (Aco,
292 IDH and OGDC) were down-accumulated (Tab. 2) (Fig. 4). These results suggest a possible
293 reduction of energy in the form of ATP generated through the oxidation of acetate derived
294 from carbohydrates lipids and proteins. The pool of NADH and precursors of certain amino
295 acids from malate and oxaloacetate could be affected.

296 In parallel to the down-accumulation of TCA cycle proteins, we observed a strong down-
297 accumulation of three components of the NADH deshydrogenase complex (NADHDH p1, p2
298 and p10) that catalyzes the transfer of electrons from NADH produced by the TCA cycle and
299 consists in the first reaction of oxidative phosphorylation (Tab. 2 & Fig. 4). An element of the
300 second reaction complex (FR(NADH)) was also down-accumulated (Tab. 2). This enzyme

reduces the fumarate in succinate and interacts with the TCA cycle. Other proteins of oxidative phosphorylation were not differentially accumulated except for one of the two gamma subunits of ATP synthase identified, which was twofold down-accumulated (Tab. 2). These results suggest a decrease of oxygenic respiration concomitant with a decrease of the TCA cycle.

Two mitochondrial import receptor subunits (TOM40 and TOM70) and five non-differentially accumulated mitochondrial import inner membrane translocase subunits (TIMs) were identified in the proteome. Whereas the TIMs were not differentially accumulated, the two TOM subunits were strongly down-accumulated in 2Xc1 (Tab. 2). In plants, TIMs and TOMs are involved in protein-import apparatus of mitochondria [76]. This suggests a decrease of mitochondrial protein import activity at receptor level.

2.6 Lipid metabolism differs at the catabolic level and the conversion of lipids to carbohydrates is drastically affected

All the enzymes for fatty acid biosynthesis from acetyl-coA were identified in the present proteome survey (Fig 4). No difference in the expression of these enzymes was observed between the two strains. Most studies on haptophytes suggest that carbon is mainly stored in the form of triacylglycerides (TAGs) or alkenones, accumulated in lipid droplets [77]. The most frequently described route to triglycerides biosynthesis is the Kennedy pathway that occurs in the endoplasmic reticulum. The four enzymes (GPAT, LPAT, PAP and DGAT) of the Kennedy pathway have been identified in the genome of *T. lutea*, but only GPAT and LPAT were detected in the proteome (Fig. 4). We recorded the strong down-accumulation of the LPAT in the 2Xc1 strain. We identified a PDAT that, in the green microalgae *Chlamydomonas reinhardtii*, catalyzes the TAGs via transacylation of diacylglycerol (DAG) with acyl groups from phospholipids, galactolipids or phosphatidylcholine (PC) [78]. These

325 authors suggest that “PDAT-mediated membrane lipid turnover is essential for membrane
326 lipid degradation with concomitant production of TAG”. The absence of DGAT detection and
327 the presence of PDAT suggests that the transfer of acyl groups from membrane lipids to DAG
328 have a predominant role to produce TAGs. The biosynthesis of alkenones is poorly described.
329 In the proteome of *T. lutea* we identified a very-long-chain 3-oxoacyl-CoA reductase (Kcr),
330 potentially involved in this biosynthesis. This protein was 2.2-fold down-accumulated in
331 2Xc1, which accordingly presents very low alkenone abundance (Tab. 3).

332 Numerous proteins involved in lipid catabolism were down-accumulated in 2Xc1 (Tab. 2).
333 These included TAGH, 3 LACS, 2 HCDH and one ACAA, all involved in the major steps of
334 β-oxidation (Fig. 4). These results suggest a strong decrease of TAG and fatty acid hydrolysis
335 machinery. The glyoxylate cycle uses acetyl-CoA from β-oxidation for biosynthesis of
336 carbohydrates by neoglucogenesis. We showed a twofold down-accumulation of ACO and the
337 strong down-accumulation of MALSH, the key enzyme of the glyoxylate cycle (Tab. 3). This
338 protein, identified by 13 peptides in the WTc1 strain, was never detected in the 2Xc1 strain.
339 All these results suggest that the conversion of lipid to carbohydrates is drastically altered in
340 2Xc1 in this experiment compared with the wild type strain.

341 ## 2.7 Carbohydrate metabolism

342 None of the unidirectional enzymes specifically involved in glycolysis or in gluconeogenesis
343 were affected in terms of abundance in this study. In haptophytes, recent studies showed that
344 carbohydrates can be stored in the form of polysaccharides and β-1,3-glucans known as
345 chrysolaminarine [79]. Little information is available on the chrysolaminarin biosynthetic
346 pathway. We identified several potential components of chrysolaminarin biosynthetic
347 pathway including PGI, PGCM, UDPGP and KRE6. The degradation of chrysolaminarin is
348 potentially catalyzed by the identified laminarinase-like protein (enzyme of the GH16 family),

by the seven identified betaglucosidases and/or by seven other glucosidases. The glucose end-product would be subsequently phosphorylated by a glucokinase (GK) before entering glycolysis. These proteins were not differentially accumulated except one lysosomal beta glucosidase, which was strongly down-accumulated in 2Xc1 (Tab. 3). Furthermore, we identified a callose synthase presumably involved in *T. lutea* cell wall polysaccharide synthesis, which was strongly up-accumulated in 2Xc1 (Tab. 3).

2.8 Metabolism of nitrogen

Nitrogen uptake includes several steps before incorporation into carbon skeletons. Nitrogen is mainly taken up in two forms: nitrate and/or ammonium (which is less costly in terms of energy). This nitrogen uptake across the plasma membrane is achieved by low or high affinity nitrate transporters (NRT) or by ammonium transporters (AMT). Nitrate is reduced to nitrite in the cytoplasm by nitrate reductase (NR). Nitrite is transported into the chloroplasts by a nitrite transporter (NAR1) for reduction to ammonia by nitrite reductase (NiR). AMT1, NRT2, NR, NAR1 and NiR were all identified in the present proteomics study. Four isoforms of NRT2 were identified in the transcriptome of *T. lutea*, but the set of 23 peptides assigned to NRT2 does not allow discrimination between these four isoforms [80]. NRT2 and AMT1 were down-accumulated in 2Xc1 (Tab. 3).

Twenty-two proteins of the catabolism of proteins, peptides and amino-acids were down-accumulated and ten were up-accumulated (Tab. 2 and3). We observed the strong up-accumulation of BCKDHA, a component of the branched-chain alpha-keto acid dehydrogenase complex involved in the second major step of the catabolism of the branched-chain amino acids (Tab. 2). The major protein periplasmic L-amino acid oxidase (PLAAOX) identified with 56 peptides was 2.2-fold down-accumulated in *T. lutea* 2Xc1 (Tab. 3). This down-accumulation was previously reported in nitrogen-starved cells from batch cultures of

373 *T. lutea* [47]. Twenty-eight proteins involved in protein degradation (proteases, peptidases
374 and proteins of proteasome complexes, ubiquitination) were differentially accumulated
375 between the two strains. An ornithine-urea cycle (OUC) driven by mitochondrial
376 carbamoylphosphate synthase (CPS) was previously suggested in haptophytes [30]. In
377 diatoms, the OUC is known to contribute to carbon and nitrogen repackaging in response to
378 changes of nitrogen availability [30]. Based on the analysis of Allen *et al*. (2011) [30], we
379 identified most of the enzymes of OUC in the proteome of *T. lutea*, including CPS, OTC,
380 Asus and AsL. Arginase, reported by Allen *et al*. (2011), was not identified in the proteome.
381 Proteins of OUC were not affected in 2Xc1 but the identified urease was twofold down-
382 accumulated in 2Xc1, suggesting a decrease of urea catabolism capacity (Tab. 3). Thirteen out
383 of the 41 identified aminoacyl-tRNA synthetases (aa-RS) were strongly down-accumulated in
384 2Xc1 (Tab. 3), suggesting a strong decrease in protein synthesis machinery.

385

386 The purpose of the Pentose Phosphate pathway (PP pathway) aims to produce ribulose-5-
387 phosphate for the synthesis of purines and pyrimidines and erythrose-4-phosphate for the
388 synthesis of aromatic amino acids. All enzymes of the pathway were identified in this
389 proteome (Fig. 4). PGCM, which catalyzes the first step, was 2.3-fold down-accumulated in
390 2Xc1 and RPPK, an essential component for the synthesis of purines and pyrimidine was
391 strongly down-accumulated (Tab. 3). These results suggest that the synthesis of nucleotides
392 and aromatic amino acids is affected in 2Xc1.

393 2.9 DNA replication and maintenance differ significantly between
394 strains'

395 The nucleotide excision repair protein RAD23 was strongly up-accumulated in *T. lutea* 2Xc1,
396 whereas the double-strand-break repair protein RAD21 and three Structural Maintenance of

Chromosomes protein (SMCs) were strongly down-accumulated. This suggests a large impact on DNA structure in 2Xc1. Twelve of the 23 identified proteins involved in replication were down-accumulated in the 2Xc1 strain (Tab. 3). This notably included the four identified DNA Replication Licensing Factors (MCM2; MCM4; MCM5; MCM6) involved in the initiation of replication.

2.10 From DNA to functional protein

More than a hundred proteins involved in transcription and splicing were identified, and the abundance of 26 was affected in 2Xc1 (Tab. 2&3). Five out of 69 initiation and transcription factors were affected in abundance in the 2Xc1 strain. Two transcription factors were strongly up-accumulated and three others were down-accumulated. This suggests that differences of transcriptional regulation level could occur between the two strains. The four identified subunits of CCR4-NOT transcription complex were down-accumulated. This protein is linked to various cellular processes including bulk mRNA degradation, miRNA-mediated repression, translational repression during translational initiation, and general transcription regulation [81]. Nine RNA helicase and polymerases out of the 28 identified were also affected in abundance in the 2Xc1 strain. Only one splicing factor of the 15 identified proteins was down-accumulated and one RNA binding protein out of the 15 identified. These results suggest that transcription is weakly affected in the 2Xc1 strain. However, the difference of accumulation of five transcription factors can be a key element in gene regulation.

Close to 200 proteins involved in translation and splicing were identified and 20 were affected in abundance in 2Xc1 (Tab. 2&3). Four of the 123 identified ribosomal proteins were up-accumulated and six were down-accumulated. Six of the 22 initiation factors and three of the elongation factors were down-accumulated.

Among the 151 proteins involved in folding and post translational modifications, we identified 36 differentially accumulated proteins, including two strongly up-accumulated isomerases, and three other up-accumulated proteins (Tab. 2&3). We also identified three down-accumulated chaperones, five down-accumulated phosphatases, one down-accumulated glucosyltransferase, six down-accumulated isomerases, and two down-accumulated proteins of ubiquitination, nine down-accumulated heat shock proteins and six down-accumulated proteins involved in oxidative stress response. These results suggest that regulation at the post translational level could strongly impact the metabolism of *T. lutea* strain 2Xc1.

2.11 Calcium signaling pathways are affected.

Six proteins containing the EF-hand calcium-binding domain were identified in the proteome. This conserved domain can be found in calcium binding proteins, or in proteins involved in the regulation of intracellular calcium level, such as calmodulin. The accumulation of all these proteins was impacted in accumulation in the 2Xc1 strain, including two up- accumulated proteins (Tab. 2) and four down- accumulated proteins (Tab. 3). In parallel, four of the five calcium/calmodulin-dependent protein kinases (CAMPK) identified in the proteome were down-accumulated (Tab. 2). In plants, these proteins are mediators of calcium signaling and involved in numerous biological functions in response to environmental changes. In chlorophyceae, calcium signaling in involved in neutral lipid accumulation [82,83]. These results suggest differences in calcium homeostasis and regulation pathways mediated by calcium between both strains.

3. Discussion

3.1 Strategy

The aim of this work was to understand the molecular mechanisms by which microalgae up-accumulate storage carbon. Most studies done until now have focused on the effect of nitrogen deficiency, which causes an accumulation of carbohydrates and then lipid storage, but also a halt in cell division that blurs the messages of metabolic analysis. In this study, we compared under identical ecophysiological conditions two strains of *T. lutea* that differ in their ability to accumulate storage lipids, without this affecting growth. The following discussion will consider the relevance of this strategy, the original behavior of strain 2Xc1 for carbon accumulation, and the strongly altered metabolism of this mutant strain revealed by our large-scale proteomics study.

We initially focused our efforts on the physiological responses of strains to nitrogen limitation at steady state, to nitrogen repletion when N/C ratio increased, and to nitrogen depletion when N/C decreased. Unlike batch cultures, continuous cultures lead to steady ecophysiological states of great interest to study signaling, tight physiological and molecular differences in microorganisms [84]. Such cultures are very appropriate for transcriptomic, proteomic and metabolomic analysis in prokaryotes and unicellular eukaryotes [85]. In our N-limited chemostat, nitrogen was continuously supplied to the photobioreactor to thereby maintain the dynamics of cell division. The high reproducibility of ecophysiological parameters at steady states and after the three spikes confirms the appropriateness of using continuous cultures to facilitate the acquisition of responsive, high-quality and reproducible data on microalgae. However, during the experiment we observed an unexpected increase of carbon assimilation capacity at steady state in the mutant strain, due to a 100% increase of carbohydrate content

after 90 days of culture at 0.5 $d^{-1,}$ (i.e. ~ 65 generations). In addition, the two strains show differences of storage lipid content at steady state, and differences in lipid degradation and accumulation kinetics in response to changes in nitrogen availability. These results are discussed below.

The proteomes of the two strains were studied to identify the differences of behavior, especially in the accumulation of storage lipids. A large number (4,332) of proteins were identified and their abundance compared between the strains. This is the first published proteome of a member of the isochrysidales and the second of a haptophyte, following the proteome of *Emiliania huxleyi* [86,87]. To our knowledge, this is the most complete proteome of a microalga published to date.

3.2 2Xc1: a plastic strain that accumulates carbohydrates and storage lipids.

Studies on chemostat are based on the principle that the growth rate is driven by the most limiting nutrient [49,88]. In such a paradigm, and without any other limitation occurring, the ability of carbon acquisition is determined by the amount of the limiting nutrient. However, when applied to long-term experiments, it does not consider the possible evolution of the studied organism. In our study, for identical limiting nitrogen quotas, a 50% increase in carbon quotas and a twofold increase of carbohydrate were measured in 2Xc1 after 3 months of continuous culture. The question of whether the plastic behavior of this strain is constant remains pending, and should be the aim of future works. The reasons that may explain a plastic phenotype are numerous and may involve adaptation and acclimation mechanisms. Similar increases of glucose content were observed in bacteria after 280 generations of glucose-limited growth in a chemostat, and was associated with multiple and stable mutations [89]. In *C. reinhardtii*, 149 single nucleotide polymorphisms resulting in amino acid

487 substitutions were observed after 1,880 generations, leading to changes of growth capacities
488 and differences in gene regulation [90]. After 65 generations, the occurrence of mutations or
489 other genomic reordering could have occurred in the 2Xc1 culture, leading to the increase of
490 carbohydrate content. Rad21 and Rad23, involved in DNA maintenance and reparation, were
491 differentially accumulated in both strains, and among the four SMCs, involved in chromatin
492 structure, three were strongly down-accumulated. The consequences could be a higher
493 genomic plasticity of the mutant strain. One drawback of the higher plasticity could be the
494 loss of this hyper-lipidic character that gives this strain its high biotechnological potential.
495 However, no such effect was observed since the isolation of this strain in 2009, which tends to
496 demonstrate the permanent character of the lipid over-accumulation in laboratory culture
497 conditions [44].

498 The nature of the carbohydrates in *T. lutea* and the involvement of the different classes of
499 carbon storage are poorly known. Identified carbohydrates of *T. lutea* such as chrysolaminarin
500 can have biotechnological interest [79,91]. We observed the up-accumulation of Callose
501 synthase in 2Xc1, suggesting that polysaccharides could be related to the increase of total
502 carbohydrates. Previous papers showed that, compared to the WT strain, the mutant strain
503 over-accumulates storage lipids in batch cultures as soon as nitrogen becomes limiting [47].
504 At steady state of this experiment in chemostat, the mutant strain limited by nitrogen
505 accumulates 2 to 3-fold more storage lipids than the WT strain and membrane lipid were quite
506 similar. Alkenones were very low in the mutant strain as previously observed [92]. The 2.2-
507 fold down-accumulated in 2Xc1 of the Very-long-chain 3-oxoacyl-CoA, putatively involved
508 in alkenone biosynthesis, could have led to the lower concentration detected. The physical
509 properties of alkenones are poorly suited to use as a biofuels but, nonetheless, represent an
510 renewable carbon feedstock [36,93].

3.3 Early response to changes of nitrogen

The dynamic model of microalgal lipid production under nitrogen limitation proposed by Mairet *et al*. (2011) [44] was used as the basis of our original hypothesis. As proposed by the model, we observed the consumption of carbohydrate and lipid storage in the mutant strain during nitrogen repletion and the accumulation of storage carbohydrate and lipids during nitrogen depletion. In most of studied microalgae, lipid accumulation occurs either at the same time or with a slight delay compared to the accumulation of carbohydrates and as consequence, lipids and carbohydrates likely compete for metabolite precursors [94]. Even if carbon allocated to lipids varies between 0.6 and 3.9% in WTc1 strain and 3.7 to 9.3% in 2Xc1 strain, the carbon allocated to carbohydrates varies between 16.2 and 37.7 % in WTc1 strain and 27.8 and 42.7% in 2Xc1 strain. This clearly reveals that in the conditions of the experiment, carbohydrates rather than storage lipids are the major and the most dynamic sink for carbon allocation in *T. lutea*. The overall measured carbohydrates are affected by changes of nitrogen availability. Conversely, the analysis of the different classes of lipids in the mutant strain suggests not a dynamic of total lipids, but rather a retroactive switch from membrane lipids to storage lipids in lipid droplets. It seems that N/C variations were too low or too short to trigger the *de novo* biosynthesis of lipids and lead to a simple initiation of storage lipid accumulation and degradation. The behavior of WTc1 was similar to 2Xc1 for carbohydrates but, surprisingly, we did not observe the same dynamic of lipid composition: (i) storage lipid accumulation was not observed in the WT strain; (ii) *de novo* biosynthesis of lipids did not seem to be activated, but changes of lipid class instead appeared from membrane lipids to lipid bodies; (iii) carbohydrate changes were observed in both strains; (iv) physiological conditions are fairly distinct from nitrogen starvation. We therefore hypothesize that what we are likely seeing is the very early stages of lipid metabolism changes in response to nitrogen

535 availability in contrast to the previous batch experiments for proteomic and transcriptomic
536 analysis [47,48].

537 In microalgae, storage lipids may serve as an internal buffer that can rapidly provide specific
538 acyl groups for new synthesis of cell membranes after N recovery [95]. TAGs appear to be
539 synthetized from the breakdown of plastid and endoplasmic reticulum membranes as well as
540 from *de novo* synthesis [96]. In *C. reinhardtii* and *Isochrysis zhangjiangensis*, TAG
541 accumulation occurs soon after nitrogen depletion, whereas the accumulation of total fatty
542 acids occurs only after chronic nitrogen starvation [13,97]. In *I. zhangjiangensis,* on the basis
543 of oleic acid incorporation into TAG, authors suggested that TAG were mainly derived from
544 freshly synthesized acyl groups. The time period of this short term response of N deprivation
545 defined by the authors (four days of nitrogen depletion) is longer than the very early short
546 term response of this study. In *T. lutea* 2Xc1 strain, storage lipid biosynthesis is swiftly
547 induced upon sudden changes in nutrient availability and membrane recycling and turnover
548 seems to be the main source of FA for TAG assembly. In other words, we suggest that in the
549 conditions of the study, TAGs are mainly synthesized from breakdown of membranes, as
550 suggested by the conversion from membrane lipids to storage lipids after changes of nitrogen
551 availability. This is supported by the non-detection of LPAT and PAP involved in *de novo*
552 TAG synthesis and by the identification of PDAT that mediates membrane lipid turnover and
553 TAG synthesis. Recently, Schmollinger *et al* (2014) [14] pinpointed the significance of
554 recycling existing thylakoid membranes for TAG production in *Chlamydomonas sp.* during
555 nitrogen starvation. Surprisingly, we did not observe a change of storage lipids in the WT
556 strain. In the conditions of this experiment, the N/C ratio varies from 0.8 to 0.13 whereas in
557 the study by Mairet *et al*. (2011) [44], lower N/C (from 0.06 to 0.09) resulted in storage lipid
558 accumulation and degradation. These results suggest that a threshold of N/C ratio likely
559 triggers accumulation and consumption of storage lipids at different levels for the two strains.

3.4 How is nitrogen limitation mediated?

The relationship between nitrogen stress and carbon metabolism has been studied mainly in the chlorophycea *Chlamydomonas reinhardtii* and the diatom *Phaeodactylum tricornutum*. Nitrogen metabolism constitutes the major sink for carbon, and N deprivation increases carbon availability for carbohydrate and lipid accumulation [13]. Although carbon reorientation mechanisms are fairly well defined in model microalgae, the signal transduction mechanisms that trigger metabolic changes in response to nitrogen limitation are very poorly understood. As previously observed by Lacour *et al*. [45], we recorded a clear negative linear correlation between nitrogen limitation of *T. lutea* grown in chemostat and carbohydrate content (Fig. 3). This suggests a quite direct signal transduction between nitrogen availability and carbohydrate metabolism. However, the differences of lipid behavior after nitrogen availability changes suggest that links between N availability and lipid metabolism are less direct and that the signalization mechanisms that differ between the strains are probably more complex. In a recent study, authors showed that Ca^{2+}-mediated signaling pathway plays a role in lipid accumulation in response to nitrogen limitation in the green algae *Chlorella. sp* [82]. Ca^{2+} is a ubiquitous intracellular second messenger in the signal transduction of environmental stimuli in plants [98]. The abundance of numerous proteins involved in Ca^{2+} signaling is strongly impacted in 2Xc1. Previous papers revealed that $Ca2^{+}$ signaling in *C. reinhardtii* and *Chlorella sp.* regulates N starvation-induced neutral lipid by increasing calmodulin activity [82,83]. We suggests that Ca^{2+} signal transduction participates in lipid accumulation in haptophytes.

It has been shown that in cells, N partitioning between proteins and RNA is driven by the N/C ratio and triggers lipid accumulation [99]. There is evidence for the remobilization and redistribution of intracellular nitrogen in 2Xc1 because of its lower content of proteins and chlorophyll (Tab. 1), the differential accumulation of proteins involved in nitrogen

585 ammonium and protein transport, in translation, in biosynthesis of purine and pyrimidine, in
586 urea catabolism and in protein degradation. This behavior resembles that of *C. reinhardtii* and
587 *P. tricornutum* when subjected to nitrogen starvation [10,11,17,100]. In 2Xc1, we observed a
588 decline in activity of protein biosynthesis with the significant decline of aminoacyl-tRNA
589 biosynthesis and also a decrease in protein and amino acid degradation. These results are
590 similar to the effects of nitrogen stress in *P. tricornutum* [101,102]. We suggest that 2Xc1
591 limits nitrogen transfers between compartments to save energy for other pathways.
592 Nevertheless, the two strains have same kinetics of nitrogen uptake after nitrogen spikes.
593 Since the accumulation of carbohydrates is strongly correlated with the N/C ratio and is
594 identical between the two strains, the mechanisms of accumulation and degradation of
595 carbohydrates appear correlated with the amount of total nitrogen in the cell. This reinforces
596 the hypothesis above of mediation between nitrogen availability and carbohydrates. With
597 regard to lipids, the 2Xc1 is more responsive to changes in N/C ratios than WTc1. Differences
598 in nitrogen partitioning, suggested by the differences of abundance of proteins involved in
599 nitrogen metabolism, could be related to the differences of lipid accumulation behavior.
600 Furthermore, the periplasmic L-amino acid oxidase (PLAAOx), and the coccolith scale
601 associated protein (CSAP1) belonged to the major proteins in abundance in the proteome of *T.*
602 *lutea* WTc1 and were down-accumulated in 2Xc1. In *T. lutea* WT, these proteins are known
603 for being co-regulated and up-accumulated during nitrogen starvation [47]. The function of
604 these proteins stays unclear and would be related to aminoacid degradation and carbon
605 homeostasis. One or both of these proteins were also up-regulated at transcript or protein level
606 in *C. reinhardtii* and *P. tricornutum* during nitrogen starvation [10,15,100]. We suggest that
607 these proteins could participate in lipid accumulation feedback repression during nitrogen
608 starvation and could participate to the control of carbon and nitrogen partitioning.

3.5 Lipid biosynthesis plays only a minor role in storage lipid up-accumulation

Enzymes of *de novo* fatty acid and TAG biosynthesis were not up-accumulated in 2Xc1. The strong down-regulation of LPAT in the 2Xc1 strain and the non-detection of two major enzymes of the Kennedy pathway suggest the presence of alternative pathways to produce TAGs in *T. lutea*. Several papers report the little or no changes in abundance of transcripts of proteins involved in fatty acid and lipid metabolism during nitrogen deprivation [7,10,13,103]. In photoautotrophically grown cells of *C reinhardtii*, precursors of fatty acid synthesis may be scarce, and are likely derived in part from the recycling of previously assimilated carbon [13]. Similarly, in heterotrophically grown cells, it is carbon precursor supply rather than the enzymes involved in fatty acid synthesis that is the limiting factor in oil synthesis under N starvation. The regulation of lipid synthesis and storage during nitrogen deprivation occurs by biochemical mechanisms dependent upon substrate levels and post-translational modifications [10]. In *P. tricornutum*, the build-up of precursors of the acetyl-CoA carboxylases may play a more significant role in TAG synthesis than the abundance of enzymes of *de novo* biosynthesis [15]. In *Isochrysis galbana*, *in vitro* activity of ACCase decreased during N starvation and increased during N recovery [104]. This suggests that the accumulation of storage lipid in cells of *Isochrysis galbana* during N starvation is more the result of the absence of cell division than the increase of lipid biosynthesis. In addition, several attempts to over-express the relevant ACCase gene in the diatoms *Cyclotella cryptica* and *Navicula saprofila*, failed to improve lipid storage, showing that lipid storage accumulation is poorly constrained by *de novo* fatty acids biosynthesis [105,106]. In *T. lutea* 2Xc1, therefore, the up-accumulation of TAG is the consequence of numerous changes of metabolism upstream or downstream of lipid biosynthesis.

3.6 Carbon partitioning optimizes TAG accumulation in 2Xc1.

In 2Xc1, proteins of TAG degradation and β-oxidation were shut down and the consequences of this bottleneck at TAGs are likely one of the main reasons for the up-accumulation of TAG in *T. lutea* 2X (Fig. 4). A previous attempt at knockdown of a multifunctional lipase / phospholipase / acyltransferase increased lipid yields in *Thalassiosira pseudonana*, without affecting the growth of this alga [107]. During TAG accumulation, genes of lipid catabolism are down regulated in *Chlorella protothecoide* and proteins down accumulated in *P tricornutum* and *Isochrysis galbana* [17,108,109]. Additionally, mutants for peroxysomal proteins of β-oxidation retain oil bodies and accumulate fatty acids in early seedling development in *Arabidopsis thaliana* [110]. In microalgae as in plants it is logical that blocking lipid degradation increases their accumulation. In 2Xc1 the decrease of lipid degradation may lead to a decrease of new acetyl-CoA provision.

In parallel, our results suggest that a decrease of acetyl-CoA should also arise from the decrease of mitochondrial oxidation of pyruvate and acetate by PDC, ACS and ALDH (Fig. 4). Plants and green algae possess a mitochondrial PDC isoform involved in supplying acetyl –CoA for the TCA cycle, and another chloroplastic PDC isoform involved in supplying acetyl–CoA for several reactions including fatty acid *de novo* synthesis (see[111]. for review). In oleaginous plants, Acetyl–CoA destined for fatty acid *de novo* synthesis is mainly produced by the PDC. On the basis of sequence homology, the conversion of pyruvate into Acetyl–CoA in *T. lutea* 2Xc1 chloroplasts appears unaffected, unlike in mitochondria; this ensures a supply of Acetyl-CoA for *de novo* biosynthesis of fatty acids.

In strictly photoautotrophic conditions, CO_2 fixation by photosynthesis is the only source or carbon for the metabolic precursors synthesis. In *C. reinhardtii*, the requirements for high amounts of energy (ATP) and reducing power (NADPH) for synthesis of storage compounds

657 are mainly provided by photosynthetic electron transport [9]. In *T. lutea* 2X, several
658 photosynthesis proteins were up-accumulated and could thus satisfy the energetic and
659 reducing power needs of carbon assimilation. In relation to photosynthesis, carbon acquisition
660 by the Calvin cycle appears to be up-activated in the 2Xc1 strain. Carbon availability is a key
661 metabolic factor controlling oil biosynthesis and carbon partitioning between carbohydrates
662 and oil. Under nitrogen limitation, *T. lutea* 2Xc1 increases its potential for lipid accumulation
663 by increasing carbon and energy availability rather than by increasing lipid biosynthesis.

664 In the paper of Song *et al* (2013) [109], the authors reported that in the haptophyte *Isochrysis*
665 *galbana* "the glycolytic pathway and citrate transport system might be the main routes for
666 lipid anabolism in N-deprived *I. galbana*, and that the tricarboxylic acid (TCA) cycle,
667 glyoxylate cycle and sulfur assimilation system might be the major pathways involved in lipid
668 catabolism" [109]. In 2Xc1, acetate and pyruvate metabolisms were impaired concomitant to
669 the shutdown of β-oxidation (Fig. 4). This may lead to a decrease of acetyl-CoA, which is the
670 precursor for TCA and glyoxylate cycles and fatty acid *de novo* biosynthesis. In fact, the key
671 enzymes of the TCA and glyoxylate cycles were strongly down-accumulated in the 2Xc1
672 strain. In the diatom *P. tricornutum*, genes coupled to β-oxidation and the TCA cycle are co-
673 regulated in the same way as observed in 2Xc1 [112]. The TCA cycle is the crossroad of
674 several central metabolic pathways. It allows the adjusted reallocation of carbon skeletons as
675 cell requirements. A reduction of TCA cycle activity results in a lower conversion from lipids
676 to carbohydrates and proteins. The pool of NADH and precursors of certain amino acids from
677 malate and oxaloacetate could be affected and could be the cause of changes in nitrogen
678 metabolism.

679 On the basis of a decrease in abundance of the proteins involved in acetyl-CoA synthesis, in
680 the TCA cycle in mitochondrial protein import machinery and in the first reactions of
681 oxidative phosphorylation, we hypothesize there is an overall decrease of mitochondrial

682 activity in the 2Xc1 (Fig. 4). In *P. tricornutum*, oxidation of FAs most likely provides acetyl-
683 CoA for the TCA cycle during dark periods [112].

684 In the model species *C. reinhardtii* and *P. tricornutum*, nitrogen starvation leads to
685 restructuration of carbon metabolism through the down-regulation of the Calvin cycle and up-
686 regulation of glycolysis, TCA cycle, and pyruvate metabolism [10,12,18]. This would support
687 the basic cellular functions during a halt in growth. It should now be asked why the cells store
688 energy-rich lipids. According to Alipanah *et al*. (2015) [18], this would lead to a funneling of
689 lipid metabolism to carbon sources. Under nitrogen limitation conditions, compared with the
690 wild strain, 2Xc1 tended to increase the Calvin cycle and limit mitochondrial activity and
691 pyruvate metabolism (Fig. 4). TCA cycle allows the optimization of carbon resources and has
692 the adaptive ability to change carbon and energy sources. We hypothesize that nitrogen-
693 limited 2Xc1 inhibits lipid catabolism and mitochondrial activity to preserve acetyl-CoA for
694 lipid anabolism and to limit carbon transfers from lipid compartments.

695 Moreover, our results show that the glyoxylate cycle in *T. lutea* 2X is shunted via the
696 shutdown at both transcriptomic and proteomic levels of the Malate synthase G. The
697 glyoxylate cycle converts acetyl-CoA to succinate for the biosynthesis of carbohydrates via
698 neoglucogenesis (Fig. 4). It is the main pathway for the synthesis of carbohydrates from fatty
699 acid oxidation. It bypasses the two reactions of the TCA cycle where four carbon molecules
700 are lost, and produces oxaloacetate which is readily utilized by gluconeogenesis for
701 carbohydrate synthesis. In *C. reinhardtii*, nitrogen deprivation results in the rapid depression
702 of glyoxylate, resulting in more available acetyl-CoA for fatty-acid biosynthesis, and sets the
703 stage for TAG biosynthesis initiation [7,10,11]. Conversely, a lipid-accumulating strain of *C.*
704 *reinhardtii* up-accumulates proteins of glyoxylate [100]. As a result the behavior of the
705 glyoxylate cycle of 2Xc1 resembles that of a nitrogen-starved alga. The shunt of glyoxylate

706 cycle is likely one of the main reason of lipid up-accumulation and high sensitivity to nitrogen
707 environment changes.

708 3.7 Conclusions

709 This study shows that the strain *T. lutea* 2Xc1 is not only very sensitive to nitrogen variations
710 in the environment, but can also increase its capacity to accumulate carbohydrates. The in-
711 depth proteomic analysis identified several mechanisms, from DNA maintenance to central
712 metabolism, that likely participate in this behavior. By comparison with nitrogen starvation,
713 which triggers TAG accumulation in algae, the lipid accumulating strain seems to behave
714 similarly to a nitrogen-starved alga for Ca^{2+} signaling, nitrogen metabolism, glyoxylate cycle
715 and lipid biosynthesis.

716 As the main result, the conversion from TAG to carbohydrates is impeded at all levels.
717 However, in contrast to nitrogen-starved algae, in the absence of a halt in growth, 2Xc1
718 appears to increase photosynthesis and carbon fixation to adjust to lipid anabolism and
719 changes in nitrogen availability. It also appears to impair mitochondrial activity to support the
720 shutdown of lipid catabolism. The key mechanisms that trigger this metabolism should occur
721 at the transcriptomic level but probably mainly occur at translational and post translational
722 levels. To conclude, this study provides significant insights into mechanisms of carbon
723 partitioning in haptophytes.

4. Material and Methods

4.1 Strains and cultures

T. lutea CCAP 927/14 wild type (WT) and mutant CCAP 927/14 (S2M2) strains previously described [46] were purified by one-cell isolation (WTc1 and 2Xc1) and maintained by batch culture in Walne's medium [113]. Both strains were grown for 85 days in chemostat at a $0.5j^{-1}$ dilution rate in modified Walne's medium containing 125/125µM N:P ratios in 10-L photobioreactors (1000 × 400 × 250 mm) illuminated with continuous light (150 $\mu mol.m^{-3}.s^{-1}$) continuously aerated by bubbling and maintained at 27°C and pH 7.3. The dilution rate was periodically checked by weighing the outcoming medium. Three nitrogen spikes were made at days 20, 43 and 83. Each spike consisted in the injection of 3,500 µmoles of $NaNO_3$ in the 10 L of culture.

4.2 Analysis

Cell Concentration (CC), Particulate Carbon (PC), Particulate Nitrogen (PN), particulate N/C ratio, Dissolved Inorganic Nitrogen (DIN) and Dissolved Inorganic Phosphorus (DIP) were assessed at high frequency (from every 2 hours to daily) throughout the course of the experiment. PC and PN were measured on a CHN-elemental analyzer. The Matlab Curve fitting toolbox was used to perform smoothing spline fitting of computed PC. A fitted model was used to calculate growth rate during the experiment. Chemical analyses of residual DIN and DIP concentrations were carried out on a DIONEX ion-chromatography system (AS9-HC column). CC was measured on a Malassez hemocytometer. Cell lipid storage per cell was estimated on the FL2 detector (488 to 585 nm) of a BD Accuri™ C6 Flow Cytometer after Nile red staining [114].

For lipid analysis, $150x10^6$ cells were filtered on 450 °C precombusted GF/C glass-fiber filters. Lipids were extracted in 6 mL chloroform/methanol (2/1, v/v) according to the method of Folch *et al*. [115] and stored at -20 °C under nitrogen. Neutral (NL) and polar lipids (PL) were analyzed separately by HPTLC on 5µl of lipid extract. All the lipid class standards and the chemicals used for HPTLC analysis were obtained from Sigma–Aldrich, at the exception of glycolipids (digalactosidediacylglyceride (DGDG), monogalactosidediacylglyceride (MGDG) and sulfoquinovosyldiacylglyceride (SQDG)), which were supplied by Larodan. HPTLC glass plates (20 × 20 mm) pre-coated with silica gel 60 were supplied by Merck. Neutral lipids were analyzed following the method described by Da Costa *et al* (2015) [92]. Six NL classes were identified / free fatty acids, sterol esters, alcohols, triacylglycerides (TAG), alkenones and free sterols : Three different HPTLC analyses were necessary to separate microalgae PL classes, These analyses followed the method used for NL but with different solvent systems / (1) methyl acetate/isopropanol/chloroform/methanol/KCl 0.25% (10/10/10/4/3.6, v/v/v/v/v), (2) methyl acetate/isopropanol/chloroform/methanol/KCl 0.25% (25/ 25/25/10/4, v/v/v/v/v) and (3) chloroform/methanol/ammonium (65/30/4, v/v/v). The first method allowed the separation of cardiolipin, lysophosphatidylcholine, phosphatidylcholine, phosphatidylserine, phosphatidylinositol,) monogalactosidediacylglycerol and digalactosidediacylglycerol (DGDG) but phosphatidylethanolamine (PE) was co-eluted with sufoquinovosyldiacylglycerol (SQDG) and phosphatidylglycerol (PG). The second method allowed isolating SQDG, whereas PE + PG were co-eluted. The third method allowed the isolation of PG whereas PE + SQDG + DGDG were co-eluted. For both NL and PL, authentic standards allowed the identification and the quantification of lipid classes. Quantification was done by scanning densitometry using winCATS software for data treatment (CAMAG, Switzerland). Results were expressed as the quantity of membrane lipids (PL + free sterols) and of storage lipids (NL - free sterols) per cell and per carbon.

771 Protein, lipid, carbohydrate and chlorophyll a measurements were converted to % of total
772 carbon using the following conversion factors: 0.53 g carbon / g proteins; 0.4 g carbon / g
773 carbohydrates; 0.76 g carbon / g lipids; 0.74 g carbon / g chlorophyll a [75].

774

775 ## 4.3 Proteomics analysis

776 In each one of both chemostats, samplings were done for proteomic analysis before each one
777 of the 3 nitrogen spikes (Pt27, Pt74, Pt117 on Fig. 1). Culture samples of 50 mL were briefly
778 centrifuged at 2,000× *g* for 5 min at 5°C and the pellet quickly frozen in liquid nitrogen and
779 conserved at -80°C for protein extractions. Total proteins were extracted and purified in the
780 presence of protease inhibitors (Complete tablets, Roche Diagnostics, Mannheim, Germany).
781 TRizol® reagent protocol was used following supplier's recommendations [116]. For each
782 extract, 80 µg proteins were pre-fractionated by 10% acrylamide SDS-PAGE. Each lane was
783 cut into 18 bands of identical size.

784 Gel bands were excised and further processed into peptides as previously described [47].
785 Resulting peptide mixtures (18 bands × 2 strains × 3 biological samples) were analyzed
786 separately by nanoscale capillary liquid chromatography-tandem mass spectrometry (LC-
787 MS/MS) using an Ultimate 3000 RSLC system (Thermo-Fisher Scientific), coupled with an
788 LTQ-Orbitrap VELOS mass spectrometer (Thermo-Fisher Scientific). Chromatographic
789 separation was conducted on a reverse-phase capillary column (Acclaim Pepmap C18 2 µm
790 100A, 75-µm i.d. × 50-cm length, Thermo-Fisher) at a flow rate of 300nL.min^{-1}. The
791 percentage of acetonitrile in the mobile phase was linearly raised from 2% up to 70% in 56
792 min. Upon elution of the peptides, full MS scans were acquired at high resolution (FWMH
793 60,000) in an Orbitrap analyzer (mass-to-charge ratio (m/z): 400 to 2,000), while collision-

induced dissociation (CID) spectra were recorded on the eight most intense ions in the linear LTQ traps.

Raw data collected during the LC-MS/MS runs were converted into the mzXML standard format using the Msconvert tool available at http://proteowizard.sourceforge.net/tools.shtml. Protein identification was performed by comparing the LC-MS/MS data against a non-redundant protein database of *T. lutea*. This database was obtained from *de novo* assembled transcriptomics data [117] as well as from *in silico* derived proteome from the *T. lutea* genome; some common contaminants including human keratins and trypsin were added to this databank (hits against these contaminants were thus discarded). The databank search engine was X!tandem (GPL v.3) embedded in the X!tandemPipeline available at http://pappso.inra.fr/bioinfo/ [118]. Enzymatic cleavage was considered as a tryptic digestion with one possible missed cleavage event. Fixed modifications of cysteine residues by iodoacetamide as well as possible oxidation of methionines were considered. Precursor mass and fragment mass tolerance were set at 5 ppm and 0.5 Da, respectively. The search results for each LC-MS/MS run were then filtered as follows: peptide-to-spectrum matches were filtered out with a p-value of 0.01. An FDR (false discovery rate) of 0.2% was achieved at the peptide level. Redundancy of protein databases was fully filtered as follows : proteins identified without specific peptides compared to others were eliminated; proteins identified with the same pool of peptides were assembled into a same subgroup; proteins were grouped by functions (identified with at least one common peptide). Protein identifications were considered as valid when at least two unique peptides and one specific peptide matched the sequence according to the above peptide requirements. An additional threshold of protein e-value was set at 10e-4. As final, the proteins identified in only one sample were eliminated.

4.4 Functional Annotation

Proteins were functionally annotated by: (1) BLAST-P against Uniprot protein databases. *e*-value of 1.0 e^{-5} and 30% identity were used as cut off. (2) Protein domain identification was done using InterProScan and NCBI Conserved Domain Database (CDD) with *e*-value threshold=0.01. A search for homologs in other microalgae was done by BLAST-P on *in silico* proteomes of the haptophyte *E. huxleyi*, the diatom *P. tricornutum* and the chlorophycea *C. reinhardtii*. Expert curation was used for validation of results and final annotation.

4.5 Quantitative proteomic analysis

Relative quantification of identified proteins was done by comparing the intensity (peak area) measured in MS for the precursor ions corresponding with unique peptides assigned to a given protein. This was achieved through XIC comparison (extracted ion chromatogram) using the MassChroQ program [119]. For each strain and each row excised from the gel lanes (1 to 18), one LC-MS/MS run among the 3 runs corresponding to the three biological samples was chosen as the "reference" for the alignment of the related peptide features. The "reference" run was that exhibiting the highest number of identified peptides. The area derived for each peptide was further normalized by the total ion current of the run, to reduce technical variability (Supp mat 6). When the same peptides were identified in different bands of SDS-PAGE lanes, their normalized areas were summed (Sum of Normalized Peptide Area). To reduce the dominance of highly ionisable peptides while keeping the variability between the samples, the SNPA of each peptide was normalized by the mean of SNPAs in biological samples. The quantity of each protein in each sample was estimated as the sum of the normalized SNPAS of its assigned peptides.

The three biological samples taken from the cultures at steady states for each strain were statistically analyzed. Missing values of non-detected proteins were replaced by the lowest

recorded value. ANOVA were performed on log2 transformed data. q-values and FDRs were calculated on the data set of *p*-values<0.05 using the package fdrtool in R software [120]. False positive were removed with a cutoff of 0.8. The difference of protein quantity between the 2 samples was expressed as the log2 fold of the means. (Log2((mean(2Xc1)/mean(WTc1)). The effect was considered significant when p<0.01 and [log2fold > 1 or < -1] or p < 0.05 and [log2fold > 2 or < -2].

References

[1] R. Sayre, Microalgae: The Potential for Carbon Capture, BioScience. 60 (2010) 722–727. doi:10.1525/bio.2010.60.9.9.

[2] O. Pulz, W. Gross, Valuable products from biotechnology of microalgae, Appl. Microbiol. Biotechnol. 65 (2004) 635–648. doi:10.1007/s00253-004-1647-x.

[3] P. Spolaore, C. Joannis-Cassan, E. Duran, A. Isambert, Commercial applications of microalgae, J. Biosci. Bioeng. 101 (2006) 87–96. doi:10.1263/jbb.101.87.

[4] W. Klinthong, A Review: Microalgae and Their Applications in CO2 Capture and Renewable Energy, Aerosol Air Qual. Res. (2015). doi:10.4209/aaqr.2014.11.0299.

[5] M. Davey, G.A. Tarran, M.M. Mills, C. Ridame, R.J. Geider, J. LaRoche, Nutrient limitation of picophytoplankton photosynthesis and growth in the tropical North Atlantic, Limnol. Oceanogr. 53 (2008) 1722–1733. doi:10.4319/lo.2008.53.5.1722.

[6] T.J. Browning, H.A. Bouman, C.M. Moore, C. Schlosser, G.A. Tarran, E.M.S. Woodward, G.M. Henderson, Nutrient regimes control phytoplankton ecophysiology in the South Atlantic, Biogeosciences. 11 (2014) 463–479. doi:10.5194/bg-11-463-2014.

[7] R. Miller, G. Wu, R. Deshpande, A. Vieler, K. Gartner, X. Li, E. Moellering, S. Zauner, A. Cornish, B. Liu, B. Bullard, B. Sears, M. Kuo, E. Hegg, Y. Shachar-Hill, S. Shiu, C. Benning, Changes in Transcript Abundance in Chlamydomonas reinhardtii following Nitrogen Deprivation Predict Diversion of Metabolism, PLANT Physiol. 154 (2010) 1737–1752. doi:10.1104/pp.110.165159.

[8] D.Y. Lee, J.-J. Park, D.K. Barupal, O. Fiehn, System Response of Metabolic Networks in Chlamydomonas reinhardtii to Total Available Ammonium, Mol. Cell. Proteomics. 11 (2012) 973–988. doi:10.1074/mcp.M111.016733.

[9] J. Fan, C. Yan, C. Andre, J. Shanklin, J. Schwender, C. Xu, Oil accumulation is controlled by carbon precursor supply for fatty acid synthesis in Chlamydomonas reinhardtii, Plant Cell Physiol. 53 (2012) 1380–1390. doi:10.1093/pcp/pcs082.

875 [10] N. Wase, P.N. Black, B.A. Stanley, C.C. DiRusso, Integrated Quantitative
876 Analysis of Nitrogen Stress Response in Chlamydomonas reinhardtii Using Metabolite and
877 Protein Profiling, J. Proteome Res. 13 (2014) 1373–1396. doi:10.1021/pr400952z.

878 [11] J.-J. Park, H. Wang, M. Gargouri, R.R. Deshpande, J.N. Skepper, F.O.
879 Holguin, M.T. Juergens, Y. Shachar-Hill, L.M. Hicks, D.R. Gang, The response of
880 Chlamydomonas reinhardtii to nitrogen deprivation: a systems biology analysis, Plant J. 81
881 (2015) 611–624. doi:10.1111/tpj.12747.

882 [12] L. Valledor, T. Furuhashi, L. Recuenco-Muñoz, S. Wienkoop, W. Weckwerth,
883 System-level network analysis of nitrogen starvation and recovery in Chlamydomonas
884 reinhardtii reveals potential new targets for increased lipid accumulation, Biotechnol.
885 Biofuels. 7 (2014) 171. doi:10.1186/s13068-014-0171-1.

886 [13] J. Msanne, D. Xu, A.R. Konda, J.A. Casas-Mollano, T. Awada, E.B. Cahoon,
887 H. Cerutti, Metabolic and gene expression changes triggered by nitrogen deprivation in the
888 photoautotrophically grown microalgae Chlamydomonas reinhardtii and Coccomyxa sp. C-
889 169, Phytochemistry. 75 (2012) 50–59. doi:10.1016/j.phytochem.2011.12.007.

890 [14] S. Schmollinger, T. Mühlhaus, N.R. Boyle, I.K. Blaby, D. Casero, T. Mettler,
891 J.L. Moseley, J. Kropat, F. Sommer, D. Strenkert, D. Hemme, M. Pellegrini, A.R. Grossman,
892 M. Stitt, M. Schroda, S.S. Merchant, Nitrogen-Sparing Mechanisms in Chlamydomonas
893 Affect the Transcriptome, the Proteome, and Photosynthetic Metabolism[W], Plant Cell. 26
894 (2014) 1410–1435. doi:10.1105/tpc.113.122523.

895 [15] J. Valenzuela, A. Mazurie, R.P. Carlson, R. Gerlach, K.E. Cooksey, B.M.
896 Peyton, M.W. Fields, Potential role of multiple carbon fixation pathways during lipid
897 accumulation in Phaeodactylum tricornutum, Biotechnol. Biofuels. 5 (2012) 40.
898 doi:10.1186/1754-6834-5-40.

899 [16] J. Valenzuela, R.P. Carlson, R. Gerlach, K. Cooksey, B.M. Peyton, B. Bothner,
900 M.W. Fields, Nutrient resupplementation arrests bio-oil accumulation in Phaeodactylum
901 tricornutum, Appl. Microbiol. Biotechnol. 97 (2013) 7049–7059. doi:10.1007/s00253-013-
902 5010-y.

903 [17] Z.-K. Yang, Y.-H. Ma, J.-W. Zheng, W.-D. Yang, J.-S. Liu, H.-Y. Li,
904 Proteomics to reveal metabolic network shifts towards lipid accumulation following nitrogen

905 deprivation in the diatom Phaeodactylum tricornutum, J. Appl. Phycol. 26 (2014) 73–82.
906 doi:10.1007/s10811-013-0050-3.

907 [18] L. Alipanah, J. Rohloff, P. Winge, A.M. Bones, T. Brembu, Whole-cell
908 response to nitrogen deprivation in the diatom Phaeodactylum tricornutum, J. Exp. Bot.
909 (2015) erv340. doi:10.1093/jxb/erv340.

910 [19] H.-P. Dong, E. Williams, D. Wang, Z.-X. Xie, R. Hsia, A. Jenck, R. Halden, J.
911 Li, F. Chen, A.R. Place, Responses of Nannochloropsis oceanica IMET1 to Long-Term
912 Nitrogen Starvation and Recovery, Plant Physiol. 162 (2013) 1110–1126.
913 doi:10.1104/pp.113.214320.

914 [20] D. Simionato, M.A. Block, N.L. Rocca, J. Jouhet, E. Maréchal, G. Finazzi, T.
915 Morosinotto, The Response of Nannochloropsis gaditana to Nitrogen Starvation Includes De
916 Novo Biosynthesis of Triacylglycerols, a Decrease of Chloroplast Galactolipids, and
917 Reorganization of the Photosynthetic Apparatus, Eukaryot. Cell. 12 (2013) 665–676.
918 doi:10.1128/EC.00363-12.

919 [21] N. Shtaida, I. Khozin-Goldberg, S. Boussiba, The role of pyruvate hub
920 enzymes in supplying carbon precursors for fatty acid synthesis in photosynthetic microalgae,
921 Photosynth. Res. 125 (2015) 407–422. doi:10.1007/s11120-015-0136-7.

922 [22] Y. Li, D. Han, G. Hu, D. Dauvillee, M. Sommerfeld, S. Ball, Q. Hu,
923 Chlamydomonas starchless mutant defective in ADP-glucose pyrophosphorylase hyper-
924 accumulates triacylglycerol, Metab. Eng. 12 (2010) 387–391.

925 [23] M. Siaut, S. Cuiné, C. Cagnon, B. Fessler, M. Nguyen, P. Carrier, A. Beyly, F.
926 Beisson, C. Triantaphylidès, Y. Li-Beisson, G. Peltier, Oil accumulation in the model green
927 alga Chlamydomonas reinhardtii: characterization, variability between common laboratory
928 strains and relationship with starch reserves, BMC Biotechnol. 11 (2011) 7.
929 doi:10.1186/1472-6750-11-7.

930 [24] H. Vigeolas, F. Duby, E. Kaymak, G. Niessen, P. Motte, F. Franck, C.
931 Remacle, Isolation and partial characterization of mutants with elevated lipid content in
932 Chlorella sorokiniana and Scenedesmus obliquus, J. Biotechnol. (2012).
933 doi:10.1016/j.jbiotec.2012.03.017.

[25] I.K. Blaby, A.G. Glaesener, T. Mettler, S.T. Fitz-Gibbon, S.D. Gallaher, B. Liu, N.R. Boyle, J. Kropat, M. Stitt, S. Johnson, C. Benning, M. Pellegrini, D. Casero, S.S. Merchant, Systems-level analysis of nitrogen starvation-induced modifications of carbon metabolism in a Chlamydomonas reinhardtii starchless mutant, Plant Cell. 25 (2013) 4305–4323. doi:10.1105/tpc.113.117580.

[26] Y.-E. Choi, H. Hwang, H.-S. Kim, J.-W. Ahn, W.-J. Jeong, J.-W. Yang, Comparative proteomics using lipid over-producing or less-producing mutants unravels lipid metabolisms in Chlamydomonas reinhardtii, Bioresour. Technol. (2013). doi:10.1016/j.biortech.2013.03.142.

[27] U. Goodenough, I. Blaby, D. Casero, S.D. Gallaher, C. Goodson, S. Johnson, J.-H. Lee, S.S. Merchant, M. Pellegrini, R. Roth, J. Rusch, M. Singh, J.G. Umen, T.L. Weiss, T. Wulan, The Path to Triacylglyceride Obesity in the sta6 Strain of Chlamydomonas reinhardtii, Eukaryot. Cell. (2014) EC.00013–14. doi:10.1128/EC.00013-14.

[28] T. Li, M. Gargouri, J. Feng, J.-J. Park, D. Gao, C. Miao, T. Dong, D.R. Gang, S. Chen, Regulation of starch and lipid accumulation in a microalga Chlorella sorokiniana, Bioresour. Technol. 180 (2015) 250–257. doi:10.1016/j.biortech.2015.01.005.

[29] B.-H. Zhu, H.-P. Shi, G.-P. Yang, N.-N. Lv, M. Yang, K.-H. Pan, Silencing UDP-glucose pyrophosphorylase gene in Phaeodactylum tricornutum affects carbon allocation, New Biotechnol. (2015). doi:10.1016/j.nbt.2015.06.003.

[30] A.E. Allen, C.L. Dupont, M. Oborník, A. Horák, A. Nunes-Nesi, J.P. McCrow, H. Zheng, D.A. Johnson, H. Hu, A.R. Fernie, C. Bowler, Evolution and metabolic significance of the urea cycle in photosynthetic diatoms, Nature. 473 (2011) 203–207. doi:10.1038/nature10074.

[31] A.E. Allen, A. Vardi, C. Bowler, An ecological and evolutionary context for integrated nitrogen metabolism and related signaling pathways in marine diatoms, Curr Opin Plant Biol. 9 (2006) 264–273. doi:10.1016/j.pbi.2006.03.013.

[32] G. Michel, T. Tonon, D. Scornet, J.M. Cock, B. Kloareg, Central and storage carbon metabolism of the brown alga Ectocarpus siliculosus: insights into the origin and evolution of storage carbohydrates in Eukaryotes, New Phytol. 188 (2010) 67–81. doi:10.1111/j.1469-8137.2010.03345.x.

964 [33] A. Sukenik, R. Wahnon, Biochemical Quality of Marine Unicellular Algae
965 with Special Emphasis on Lipid-Composition .1. Isochrysis-Galbana, Aquaculture. 97 (1991)
966 61–72. doi:10.1016/0044-8486(91)90279-G.

967 [34] M.L. Eltgroth, R.L. Watwood, G.V. Wolfe, Production and cellular localization
968 of neutral long chain lipids in the haptophyte algae Isochrysis galbana and Emiliania huxleyi,
969 J. Phycol. 41 (2005) 1000–1009. doi:10.1111/j.1529-8817.2005.00128.x.

970 [35] E.M. Bendif, I. Probert, D.C. Schroeder, C. de Vargas, On the description of
971 Tisochrysis lutea gen. nov. sp. nov. and Isochrysis nuda sp. nov. in the Isochrysidales, and the
972 transfer of Dicrateria to the Prymnesiales (Haptophyta), J. Appl. Phycol. 25 (2013) 1763–
973 1776. doi:10.1007/s10811-013-0037-0.

974 [36] I.T. Marlowe, J.C. Green, A.C. Neal, S.C. Brassell, G. Eglinton, P.A. Course,
975 Long chain (n-C37–C39) alkenones in the Prymnesiophyceae. Distribution of alkenones and
976 other lipids and their taxonomic significance, Br. Phycol. J. 19 (1984) 203–216.
977 doi:10.1080/00071618400650221.

978 [37] H. Liu, I. Probert, J. Uitz, H. Claustre, S. Aris-Brosou, M. Frada, F. Not, C. de
979 Vargas, Extreme diversity in noncalcifying haptophytes explains a major pigment paradox in
980 open oceans, Proc. Natl. Acad. Sci. 106 (2009) 12803–12808. doi:10.1073/pnas.0905841106.

981 [38] E. Fernández, E. Marañón, W.M. Balch, Intracellular carbon partitioning in the
982 coccolithophorid Emiliania huxleyi, J. Mar. Syst. 9 (1996) 57–66. doi:10.1016/0924-
983 7963(96)00016-4.

984 [39] Y. Tsuji, M. Yamazaki, I. Suzuki, Y. Shiraiwa, Quantitative Analysis of
985 Carbon Flow into Photosynthetic Products Functioning as Carbon Storage in the Marine
986 Coccolithophore, Emiliania huxleyi, Mar. Biotechnol. 17 (2015) 428–440.
987 doi:10.1007/s10126-015-9632-1.

988 [40] S.J. Finch, The Effects of Nitrogen Source on the Physiology and Primary
989 Productivity of the Coccolithophorid Emiliania Huxleyi, J. Phycol. 47 (2011) S26–S26.

990 [41] L.A. Meireles, A.C. Guedes, F.X. Malcata, Lipid class composition of the
991 microalga Pavlova lutheri: eicosapentaenoic and docosahexaenoic acids, J. Agric. Food
992 Chem. 51 (2003) 2237–2241. doi:10.1021/jf025952y.

993 [42] E. Ryckebosch, C. Bruneel, R. Termote-Verhalle, K. Goiris, K. Muylaert, I.
994 Foubert, Nutritional evaluation of microalgae oils rich in omega-3 long chain polyunsaturated
995 fatty acids as an alternative for fish oil, Food Chem. 160 (2014) 393–400.
996 doi:10.1016/j.foodchem.2014.03.087.

997 [43] G. Bougaran, O. Bernard, A. Sciandra, Modeling continuous cultures of
998 microalgae colimited by nitrogen and phosphorus, J. Theor. Biol. 265 (2010) 443–454.
999 doi:10.1016/j.jtbi.2010.04.018.

1000 [44] F. Mairet, O. Bernard, P. Masci, T. Lacour, A. Sciandra, Modelling neutral
1001 lipid production by the microalga Isochrysis aff. galbana under nitrogen limitation, Bioresour.
1002 Technol. 102 (2011) 142–149. doi:10.1016/j.biortech.2010.06.138.

1003 [45] T. Lacour, A. Sciandra, A. Talec, P. Mayzaud, O. Bernard, Neutral lipids and
1004 carbohydrate productivities as a response to nitrogen status in Isochrysis sp. (T-Iso,
1005 haptophyceae):Starvation versus limitation, J. Phycol. 48 (2012) 647–656.
1006 doi:10.1111/j.1529-8817.2012.01154.x.

1007 [46] G. Bougaran, C. Rouxel, N. Dubois, R. Kaas, S. Grouas, E. Lukomska, J.-R.
1008 Le Coz, J.-P. Cadoret, Enhancement of neutral lipid productivity in the microalga Isochrysis
1009 affinis Galbana (T-Iso) by a mutation-selection procedure, Biotechnol. Bioeng. 109 (2012)
1010 2737–2745. doi:10.1002/bit.24560.

1011 [47] M. Garnier, G. Carrier, H. Rogniaux, E. Nicolau, G. Bougaran, B. Saint-Jean,
1012 J.P. Cadoret, Comparative proteomics reveals proteins impacted by nitrogen deprivation in
1013 wild-type and high lipid-accumulating mutant strains of Tisochrysis lutea, J. Proteomics. 105
1014 (2014) 107–120. doi:10.1016/j.jprot.2014.02.022.

1015 [48] G. Carrier, M. Garnier, L. Le Cunff, G. Bougaran, I. Probert, C. De Vargas, E.
1016 Corre, J.-P. Cadoret, B. Saint-Jean, Comparative Transcriptome of Wild Type and Selected
1017 Strains of the Microalgae Tisochrysis lutea Provides Insights into the Genetic Basis, Lipid
1018 Metabolism and the Life Cycle, PLoS ONE. 9 (2014) e86889.
1019 doi:10.1371/journal.pone.0086889.

1020 [49] M.R. Droop, The nutrient status of algal cells in continuous culture, J. Mar.
1021 Biol. Assoc. U. K. 54 (1974) 825–855. doi:10.1017/S002531540005760X.

[50] G. Fu, C. Nagasato, S. Oka, J.M. Cock, T. Motomura, Proteomics Analysis of Heterogeneous Flagella in Brown Algae (Stramenopiles), Protist. 165 (2014) 662–675. doi:10.1016/j.protis.2014.07.007.

[51] V. Wagner, J. Boesger, M. Mittag, Sub-proteome analysis in the green flagellate alga Chlamydomonas reinhardtii, J. BASIC Microbiol. 49 (2009) 32–41. doi:10.1002/jobm.200800292.

[52] S. Wang, Q. Hu, M. Sommerfeld, F. Chen, Cell wall proteomics of the green alga Haematococcus pluvialis (Chlorophyceae), PROTEOMICS. 4 (2004) 692–708. doi:10.1002/pmic.200300634.

[53] K. van Wijk, Plastid proteomics, PLANT Physiol. Biochem. 42 (2004) 963–977. doi:10.1016/j.plaphy.2004.10.015.

[54] C. Ji, X. Cao, H. Liu, J. Qu, C. Yao, H. Zou, S. Xue, Investigating Cellular Responses During Photohydrogen Production by the Marine Microalga Tetraselmis subcordiformis by Quantitative Proteome Analysis, Appl. Biochem. Biotechnol. 177 (2015) 649–661. doi:10.1007/s12010-015-1769-x.

[55] F.V. Winck, D.O. Páez Melo, A.F. González Barrios, Carbon acquisition and accumulation in microalgae Chlamydomonas: Insights from “omics” approaches, J. Proteomics. 94 (2013) 207–218. doi:10.1016/j.jprot.2013.09.016.

[56] D. Nojima, T. Yoshino, Y. Maeda, M. Tanaka, M. Nemoto, T. Tanaka, Proteomics Analysis of Oil Body-Associated Proteins in the Oleaginous Diatom, J. Proteome Res. 12 (2013) 5293–5301. doi:10.1021/pr4004085.

[57] R.N. Carvalho, T. Lettieri, Proteomic analysis of the marine diatom Thalassiosira pseudonana upon exposure to benzo(a)pyrene, BMC Genomics. 12 (2011) 159. doi:10.1186/1471-2164-12-159.

[58] A.X. Yi, P.T.Y. Leung, K.M.Y. Leung, Photosynthetic and molecular responses of the marine diatom Thalassiosira pseudonana to triphenyltin exposure, Aquat. Toxicol. 154 (2014) 48–57. doi:10.1016/j.aquatox.2014.05.004.

1049 [59] S. Gillet, P. Decottignies, S. Chardonnet, P. Le Marechal, Cadmium response
1050 and redoxin targets in Chlamydomonas reinhardtii: a proteomic approach, Photosynth. Res.
1051 89 (2006) 201–211. doi:10.1007/s11120-006-9108-2.

1052 [60] S. Wang, F. Chen, M. Sommerfeld, Q. Hu, Proteomic analysis of molecular
1053 response to oxidative stress by the green alga Haematococcus pluvialis (Chlorophyceae),
1054 PLANTA. 220 (2004) 17–29. doi:10.1007/s00425-004-1323-5.

1055 [61] T. Nosenko, K. Lidie, F. Van Dolah, E. Lindquist, J. Cheng, D. Bhattacharya,
1056 Chimeric plastid proteome in the florida “red tide” dinoflagellate Karenia brevis, Mol. Biol.
1057 Evol. 23 (2006) 2026–2038. doi:10.1093/molbev/msl074.

1058 [62] M.A. Minge, K. Shalchian-Tabrizi, O.K. Tørresen, K. Takishita, I. Probert, Y.
1059 Inagaki, D. Klaveness, K.S. Jakobsen, A phylogenetic mosaic plastid proteome and unusual
1060 plastid-targeting signals in the green-colored dinoflagellate Lepidodinium chlorophorum,
1061 BMC Evol. Biol. 10 (2010) 191. doi:10.1186/1471-2148-10-191.

1062 [63] L. Valledor, L. Recuenco-Munoz, V. Egelhofer, S. Wienkoop, W. Weckwerth,
1063 The different proteomes of Chlamydomonas reinhardtii, J. Proteomics. 75 (2012) 5883–5887.
1064 doi:10.1016/j.jprot.2012.07.045.

1065 [64] H.M. Nguyen, M. Baudet, S. Cuiné, J.-M. Adriano, D. Barthe, E. Billon, C.
1066 Bruley, F. Beisson, G. Peltier, M. Ferro, Y. Li-Beisson, Proteomic profiling of oil bodies
1067 isolated from the unicellular green microalga Chlamydomonas reinhardtii: with focus on
1068 proteins involved in lipid metabolism, Proteomics. 11 (2011) 4266–4273.
1069 doi:10.1002/pmic.201100114.

1070 [65] B.K. Ndimba, R.J. Ndimba, T.S. Johnson, R. Waditee-Sirisattha, M. Baba, S.
1071 Sirisattha, Y. Shiraiwa, G.K. Agrawal, R. Rakwal, Biofuels as a sustainable energy source:
1072 An update of the applications of proteomics in bioenergy crops and algae, J. Proteomics. 93
1073 (2013) 234–244. doi:10.1016/j.jprot.2013.05.041.

1074 [66] J. Kim, W. Lee, B. Kim, C. Lee, Proteomic analysis of protein expression
1075 patterns associated with astaxanthin accumulation by green alga Haematococcus pluvialis
1076 (Chlorophyceae) under high light stress, J. Microbiol. Biotechnol. 16 (2006) 1222–1228.

[67] N. Tran, J. Park, S. Hong, C. Lee, Proteomics of proteins associated with astaxanthin accumulation in the green algae Haematococcus lacustris under the influence of sodium orthovanadate, Biotechnol. Lett. 31 (2009) 1917–1922. doi:10.1007/s10529-009-0095-1.

[68] L.L. Wurch, E.M. Bertrand, M.A. Saito, B.A.S. Van Mooy, S.T. Dyhrman, Proteome Changes Driven by Phosphorus Deficiency and Recovery in the Brown Tide-Forming Alga Aureococcus anophagefferens, PLoS ONE. 6 (2011) e28949. doi:10.1371/journal.pone.0028949.

[69] S.T. Dyhrman, B.D. Jenkins, T.A. Rynearson, M.A. Saito, M.L. Mercier, H. Alexander, L.P. Whitney, A. Drzewianowski, V.V. Bulygin, E.M. Bertrand, Z. Wu, C. Benitez-Nelson, A. Heithoff, The Transcriptome and Proteome of the Diatom Thalassiosira pseudonana Reveal a Diverse Phosphorus Stress Response, PLoS ONE. 7 (2012) e33768. doi:10.1371/journal.pone.0033768.

[70] S. Wang, X. Shi, B. Palenik, Characterization of Picochlorum sp. use of wastewater generated from hydrothermal liquefaction as a nitrogen source, Algal Res. 13 (2016) 311–317. doi:10.1016/j.algal.2015.11.015.

[71] E.C. Goncalves, J. Koh, N. Zhu, M.-J. Yoo, S. Chen, T. Matsuo, J.V. Johnson, B. Rathinasabapathi, Nitrogen starvation-induced triacylglycerol accumulation in the green algae: Evidence for a role for ROC40, a transcription factor involved in circadian rhythm, Plant J. (2016) n/a–n/a. doi:10.1111/tpj.13144.

[72] X. Bai, H. Song, M. Lavoie, K. Zhu, Y. Su, H. Ye, S. Chen, Z. Fu, H. Qian, Proteomic analyses bring new insights into the effect of a dark stress on lipid biosynthesis in Phaeodactylum tricornutum, Sci. Rep. 6 (2016) 25494. doi:10.1038/srep25494.

[73] Q. Shi, H. Araie, R.K. Bakku, Y. Fukao, R. Rakwal, I. Suzuki, Y. Shiraiwa, Proteomic analysis of lipid body from the alkenone-producing marine haptophyte alga Tisochrysis lutea, PROTEOMICS. (2015) n/a–n/a. doi:10.1002/pmic.201500010.

[74] N.D. Romanova, A.F. Sazhin, Relationships between the cell volume and the carbon content of bacteria, Oceanology. 50 (2010) 522–530. doi:10.1134/S0001437010040089.

[75] R. Geider, J. La Roche, Redfield revisited: variability of C:N:P in marine microalgae and its biochemical basis, Eur. J. Phycol. 37 (2002) 1–17. doi:10.1017/S0967026201003456.

[76] H.-P. Braun, U.K. Schmitz, The protein-import apparatus of plant mitochondria, Planta. 209 (1999) 267–274. doi:10.1007/s004250050632.

[77] J. Shi, B. Podola, M. Melkonian, Application of a prototype-scale Twin-Layer photobioreactor for effective N and P removal from different process stages of municipal wastewater by immobilized microalgae, Bioresour. Technol. 154 (2014) 260–266. doi:10.1016/j.biortech.2013.11.100.

[78] K. Yoon, D. Han, Y. Li, M. Sommerfeld, Q. Hu, Phospholipid:diacylglycerol acyltransferase is a multifunctional enzyme involved in membrane lipid turnover and degradation while synthesizing triacylglycerol in the unicellular green microalga Chlamydomonas reinhardtii, Plant Cell. 24 (2012) 3708–3724. doi:10.1105/tpc.112.100701.

[79] I. Sadovskaya, A. Souissi, S. Souissi, T. Grard, P. Lencel, C.M. Greene, S. Duin, P.S. Dmitrenok, A.O. Chizhov, A.S. Shashkov, A.I. Usov, Chemical structure and biological activity of a highly branched (1 → 3,1 → 6)-β-d-glucan from Isochrysis galbana, Carbohydr. Polym. 111 (2014) 139–148. doi:10.1016/j.carbpol.2014.04.077.

[80] A. Charrier, J.-B. Bérard, G. Bougaran, G. Carrier, E. Lukomska, N. Schreiber, F. Fournier, A.F. Charrier, C. Rouxel, M. Garnier, J.-P. Cadoret, B. Saint-Jean, High-affinity nitrate/nitrite transporter genes (Nrt2) in Tisochrysis lutea: identification and expression analyses reveal some interesting specificities of Haptophyta microalgae, Physiol. Plant. 154 (2015) 572–590. doi:10.1111/ppl.12330.

[81] X. Zheng, R. Dumitru, B.L. Lackford, J.M. Freudenberg, A.P. Singh, T.K. Archer, R. Jothi, G. Hu, Cnot1, Cnot2, and Cnot3 maintain mouse and human ESC identity and inhibit extraembryonic differentiation, Stem Cells Dayt. Ohio. 30 (2012) 910–922. doi:10.1002/stem.1070.

[82] H. Chen, Y. Zhang, C. He, Q. Wang, Ca2+ Signal Transduction Related to Neutral Lipid Synthesis in an Oil-Producing Green Alga Chlorella sp. C2, Plant Cell Physiol. 55 (2014) 634–644. doi:10.1093/pcp/pcu015.

[83] H. Chen, J. Hu, Y. Qiao, W. Chen, J. Rong, Y. Zhang, C. He, Q. Wang, Ca2+-regulated cyclic electron flow supplies ATP for nitrogen starvation-induced lipid biosynthesis in green alga, Sci. Rep. 5 (2015) 15117. doi:10.1038/srep15117.

[84] P.A. Hoskisson, G. Hobbs, Continuous culture – making a comeback?, Microbiology. 151 (2005) 3153–3159. doi:10.1099/mic.0.27924-0.

[85] A.T. Bull, The renaissance of continuous culture in the post-genomics age, J. Ind. Microbiol. Biotechnol. 37 (2010) 993–1021. doi:10.1007/s10295-010-0816-4.

[86] B.M. Jones, R.J. Edwards, P.J. Skipp, C.D. O'Connor, M.D. Iglesias-Rodriguez, Shotgun Proteomic Analysis of Emiliania huxleyi, a Marine Phytoplankton Species of Major Biogeochemical Importance, Mar. Biotechnol. (2010). doi:10.1007/s10126-010-9320-0.

[87] B.A. McKew, S.C. Lefebvre, E.P. Achterberg, G. Metodieva, C.A. Raines, M.V. Metodiev, R.J. Geider, Plasticity in the proteome of Emiliania huxleyi CCMP 1516 to extremes of light is highly targeted, New Phytol. 200 (2013) 61–73. doi:10.1111/nph.12352.

[88] G.-Y. Rhee, Effects of N:P atomic ratios and nitrate limitation on algal growth, cell composition, and nitrate uptake 1, Limnol. Oceanogr. 23 (1978) 10–25. doi:10.4319/lo.1978.23.1.0010.

[89] L. Notley-McRobb, T. Ferenci, The generation of multiple co-existing mal-regulatory mutations through polygenic evolution in glucose-limited populations of Escherichia coli, Environ. Microbiol. 1 (1999) 45–52. doi:10.1046/j.1462-2920.1999.00003.x.

[90] M.-M. Perrineau, J. Gross, E. Zelzion, D.C. Price, O. Levitan, J. Boyd, D. Bhattacharya, Using Natural Selection to Explore the Adaptive Potential of Chlamydomonas reinhardtii, PLoS ONE. 9 (2014) e92533. doi:10.1371/journal.pone.0092533.

[91] Y. Sun, H. Wang, G. Guo, Y. Pu, B. Yan, The isolation and antioxidant activity of polysaccharides from the marine microalgae Isochrysis galbana, Carbohydr. Polym. 113 (2014) 22–31. doi:10.1016/j.carbpol.2014.06.058.

[92] F. Da Costa, B. Petton, C. Mingant, G. Bougaran, C. Rouxel, C. Quéré, G. h. Wikfors, P. Soudant, R. Robert, Influence of one selected Tisochrysis lutea strain rich in

1163 lipids on Crassostrea gigas larval development and biochemical composition, Aquac. Nutr.
1164 (2015) n/a–n/a. doi:10.1111/anu.12301.

1165 [93] G.W. O'Neil, C.A. Carmichael, T.J. Goepfert, J.M. Fulton, G. Knothe, C.P.L.
1166 Lau, S.R. Lindell, N.G.-E. Mohammady, B.A.S. Van Mooy, C.M. Reddy, Beyond Fatty Acid
1167 Methyl Esters: Expanding the Renewable Carbon Profile with Alkenones from Isochrysis sp.,
1168 Energy Fuels. 26 (2012) 2434–2441.

1169 [94] H.-T. Wang, C.-H. Yao, J.-N. Ai, X.-P. Cao, S. Xue, W. Wang, Identification
1170 of carbohydrates as the major carbon sink of the marine microalga Isochrysis zhangjiangensis
1171 (Haptophyta) and optimization of its productivity by nitrogen manipulation, Bioresour.
1172 Technol. (2014). doi:10.1016/j.biortech.2014.08.090.

1173 [95] I. Khozin-Goldberg, P. Shrestha, Z. Cohen, Mobilization of arachidonyl
1174 moieties from triacylglycerols into chloroplastic lipids following recovery from nitrogen
1175 starvation of the microalga Parietochloris incisa, Biochim. Biophys. Acta BBA - Mol. Cell
1176 Biol. Lipids. 1738 (2005) 63–71. doi:10.1016/j.bbalip.2005.09.005.

1177 [96] M.T. Guarnieri, A. Nag, S.L. Smolinski, A. Darzins, M. Seibert, P.T. Pienkos,
1178 Examination of triacylglycerol biosynthetic pathways via de novo transcriptomic and
1179 proteomic analyses in an unsequenced microalga, PloS One. 6 (2011) e25851.
1180 doi:10.1371/journal.pone.0025851.

1181 [97] H.-T. Wang, Y.-Y. Meng, X.-P. Cao, J.-N. Ai, J.-N. Zhou, S. Xue, W. Wang,
1182 Coordinated response of photosynthesis, carbon assimilation, and triacylglycerol
1183 accumulation to nitrogen starvation in the marine microalgae Isochrysis zhangjiangensis
1184 (Haptophyta), Bioresour. Technol. 177 (2015) 282–288. doi:10.1016/j.biortech.2014.11.028.

1185 [98] N. Tuteja, S. Mahajan, Calcium Signaling Network in Plants, Plant Signal.
1186 Behav. 2 (2007) 79–85.

1187 [99] C. Adams, B. Bugbee, Nitrogen retention and partitioning at the initiation of
1188 lipid accumulation in nitrogen-deficient algae, J. Phycol. 50 (2014) 356–365.
1189 doi:10.1111/jpy.12167.

1190 [100] N. Velmurugan, M. Sung, S.S. Yim, M.S. Park, J.W. Yang, K.J. Jeong,
1191 Systematically programmed adaptive evolution reveals potential role of carbon and nitrogen

pathways during lipid accumulation in Chlamydomonas reinhardtii, Biotechnol. Biofuels. 7 (2014) 117. doi:10.1186/s13068-014-0117-7.

[101] T. Mock, M.P. Samanta, V. Iverson, C. Berthiaume, M. Robison, K. Holtermann, C. Durkin, S.S. BonDurant, K. Richmond, M. Rodesch, T. Kallas, E.L. Huttlin, F. Cerrina, M.R. Sussman, E.V. Armbrust, Whole-genome expression profiling of the marine diatom Thalassiosira pseudonana identifies genes involved in silicon bioprocesses, Proc. Natl. Acad. Sci. U. S. A. 105 (2008) 1579–1584. doi:10.1073/pnas.0707946105.

[102] N.L. Hockin, T. Mock, F. Mulholland, S. Kopriva, G. Malin, The Response of Diatom Central Carbon Metabolism to Nitrogen Starvation Is Different from That of Green Algae and Higher Plants, Plant Physiol. 158 (2012) 299–312. doi:10.1104/pp.111.184333.

[103] E. Moellering, C. Benning, RNA Interference Silencing of a Major Lipid Droplet Protein Affects Lipid Droplet Size in Chlamydomonas reinhardtii, Eukaryot. CELL. 9 (2010) 97–106. doi:10.1128/EC.00203-09.

[104] A. Livne, A. Sukenik, Lipid Synthesis and Abundance of Acetyl CoA Carboxylase in *Isochrysis galbana* (Prymnesiophyceae) Following Nitrogen Starvation, Plant Cell Physiol. 33 (1992) 1175–1181.

[105] T. Dunahay, E. Jarvis, S. Dais, P. Roessler, Manipulation of microalgal lipid production using genetic engineering, Appl. Biochem. Biotechnol. 57-8 (1996) 223–231.

[106] J. Sheehan, T.G. Dunahay, J. Benemann, P. Roessler, A Look back at the U.S Department of Energy's Aquatic Species Program : Biodiesel from Algae (1998).

[107] E.M. Trentacoste, R.P. Shrestha, S.R. Smith, C. Glé, A.C. Hartmann, M. Hildebrand, W.H. Gerwick, Metabolic engineering of lipid catabolism increases microalgal lipid accumulation without compromising growth, Proc. Natl. Acad. Sci. 110 (2013) 19748–19753. doi:10.1073/pnas.1309299110.

[108] Y. Li, Z. Yuan, J. Mu, D. Chen, B. Feng, Proteomic Analysis of Lipid Accumulation in Chlorella protothecoides Cells by Heterotrophic N Deprivation Coupling Cultivation, Energy Fuels. 27 (2013) 4031–4040. doi:10.1021/ef4000177.

[109] P. Song, L. Li, J. Liu, Proteomic Analysis in Nitrogen-Deprived Isochrysis galbana during Lipid Accumulation, PLoS ONE. 8 (2013) e82188. doi:10.1371/journal.pone.0082188.

[110] G. Cassin-Ross, J. Hu, Systematic Phenotypic Screen of Arabidopsis Peroxisomal Mutants Identifies Proteins Involved in β-Oxidation, Plant Physiol. 166 (2014) 1546–1559. doi:10.1104/pp.114.250183.

[111] N. Shtaida, I. Khozin-Goldberg, S. Boussiba, The role of pyruvate hub enzymes in supplying carbon precursors for fatty acid synthesis in photosynthetic microalgae, Photosynth. Res. 125 (2015) 407–422. doi:10.1007/s11120-015-0136-7.

[112] A. Mühlroth, K. Li, G. Røkke, P. Winge, Y. Olsen, M.F. Hohmann-Marriott, O. Vadstein, A.M. Bones, Pathways of Lipid Metabolism in Marine Algae, Co-Expression Network, Bottlenecks and Candidate Genes for Enhanced Production of EPA and DHA in Species of Chromista, Mar. Drugs. 11 (2013) 4662–4697. doi:10.3390/md11114662.

[113] P.R Walne, Experiments in the large scale culture of the larvae of Ostrea edulis. L, FISH INVEST MINISTR, 1996.

[114] P. Greenspan, E. Mayer, S. Fowler, Nile Red - a Selective Fluorescent Stain for Intracellular Lipid Droplets, J. Cell Biol. 100 (1985) 965–973. doi:10.1083/jcb.100.3.965.

[115] J. Folch, M. Lees, G.H.S. Stanley, A Simple Method for the Isolation and Purification of Total Lipides from Animal Tissues, J. Biol. Chem. 226 (1957) 497–509.

[116] A.B. Hummon, S.R. Lim, M.J. Difilippantonio, T. Ried, Isolation and solubilization of proteins after TRIzol extraction of RNA and DNA from patient material following prolonged storage, BioTechniques. 42 (2007) 467–470, 472.

[117] J.-P. Cadoret, G. Bougaran, J.-B. Bérard, G. Carrier, A. Charrier, N. Coulombier, M. Garnier, R. Kaas, L. Le Déan, E. Lukomska, E. Nicolau, C. Rouxel, B. Saint-Jean, N. Schreiber, Microalgae and Biotechnology, in: A. Monaco, P. Prouzet (Eds.), Dev. Mar. Resour., John Wiley & Sons, Inc., 2014: pp. 57–115.

[118] R. Craig, R.C. Beavis, TANDEM: matching proteins with tandem mass spectra, Bioinforma. Oxf. Engl. 20 (2004) 1466–1467. doi:10.1093/bioinformatics/bth092.

[119] B. Valot, O. Langella, E. Nano, M. Zivy, MassChroQ: A versatile tool for mass spectrometry quantification, Proteomics. 11 (2011) 3572–3577. doi:10.1002/pmic.201100120.

[120] J.D. Storey, R. Tibshirani, Statistical significance for genomewide studies, Proc. Natl. Acad. Sci. 100 (2003) 9440–9445. doi:10.1073/pnas.1530509100.

Abbreviations

ACAA : 3-ketoacyl-CoA thiolase ; ACCase : Acetyl-CoA carboxylase ; ACO : Aconitase ; ACS : Acetyl-coenzyme A synthetase ; ALDH : Acetaldehyde dehydrogenase ; BC1-1 : Cytochrome b-c1 complex subunit ; CCP : Cytochrome c peroxidase ; Cox : Cytochrome c oxidase ; CS : Citrate synthase ; CyC6 : Cytochrome c6 ; Cyt-c : Cytochrome c ; DGAT : Diacylglycerol O-acyltransferase ; EAR : Enoyl-[acyl-carrier-protein] reductase 1 ; Eno : Enolase ; FBPA : Fructose-bisphosphate aldolase ; FBPase : Chloroplastic Fructose-1,6-bisphosphatase 1 ; Fd : Ferredoxin ; FNR : Ferredoxin--NADP reductase ; FR : Fumarate reductase ; Fum : Fumarase ; G6P-I : Putative glucose-6-phosphate 1-epimerase ; GAPDH : glyceraldehyde-3-phosphate dehydrogenase ; GDH : Glycine dehydrogenase ; GPAT : glycerol-3-phosphate acyltransferase ; HAD : 3-hydroxyacyl-[acyl-carrier-protein] dehydratase ; HCDH : 3-hydroxyacyl-CoA dehydrogenase ; HK : Hexokinase ; ICL : Isocitrate lyase ; IDH : Isocitrate dehydrogenase [NADP] ; KAR : 3-oxoacyl-[acyl-carrier-protein] reductase ; KASII : 3-oxoacyl-[acyl-carrier-protein] synthase ; LACS : Long chain acyl-CoA synthetase ; LPAAT : lysophosphatidic acid-acyltransferase ; MALsH : Malate synthase ; MAT : Malonyl-CoA-acyl carrier protein transacylase ; MDH : Malate dehydrogenase ; ME1 : NADP-dependent malic enzyme ; NADHDH : NADH dehydrogenase ; OGDC-E2 : 2-oxoglutarate dehydrogenase-E2 ; PAP : Phosphatidic acid phosphatase ; PCr : pyruvate carboxylase ; PDAT : phospholipid:diacylglycerol acyltransferase ; PDC : Pyruvate Deshydrogenase Complex PDC-E1-a/ß ; PDHK : Pyruvate dehydrogenase kinase ; PeB : Cytochrome b6 ; PEPCK : Phosphoenolpyruvate carboxykinase [ATP] ; PetA : Apocytochrome f ; PFK : 6-phosphofructokinase ; PGAM : 2,3-bisphosphoglycerate-dependent phosphoglycerate mutase ; PGCM : phosphoglucomutase ; PGD : 6-phosphogluconate dehydrogenase ; PGI : Glucose-6-phosphate isomerase ; PGK :

Phosphoglycerate kinase ; PGM : Phosphoglucomutase ; PK : Pyruvate kinase ; PPE : Pentose-5-phosphate 3-épimérase ; PPK : Phosphoribulokinase ; PsaA : Photosystem I P700 chlorophyll a apoprotein ; PsaB : Photosystem I P700 chlorophyll a apoprotein A2 ; PsaL : Photosystem I reaction center subunit XI ; PsbB : Photosystem II protein ; PsYcf3 : Photosystem I assembly protein ; RbcS : Ribulose bisphosphate carboxylase small chain ; Rieske : Cytochrome b6-f complex iron-sulfur subunit ; RPEh : D-Ribulose-5-Phosphate 3-Epimerase ; RPI : Probable ribose-5-phosphate isomerase ; RPPK : Ribose-phosphate pyrophosphokinase ; SDH : Succinate dehydrogenase ; STK : succinyl-CoA ligase ; TAGH : Triacylglycerol hydrolase ; TAL : Transaldolase ; TK : Transketolase ; TPI : Triosephosphate isomerase.

Legends

Fig. 1: Computed ecophysiological parameters. WTc1 and 2Xc1 strains were cultured for 85 days in nitrogen limited chemostats subjected to three nitrogen spikes. Cell Concentration (CC), Dissolved Inorganic Nitrogen (DIN) (squares) and Dissolved Inorganic Phosphorus (DIP) (no square), Particulate Carbon (PC), Particulate Nitrogen (PN), and particulate N/C ratio were calculated. Three steady states were delimited. SS1: Day 10→D20, SS2: D30→D43, and SS3: D50→D80. N/C ratio computed after the first N spike zooms in on the bottom square. Three phases were delimited: (1) N limitation, (2) N repletion and (3) N depletion.

Fig. 2: Lipid and carbohydrate analysis during different phases before and after each N spike. (1) N limitation, (2) N repletion and (3) N depletion. Computing of N/C ratios, storage and membrane lipids by HPTLC, and total carbohydrates. Computing of storage lipids by Nile red fluorescence after the first N spike is given in the right-hand box.

Fig. 3: Proteomic analysis: (A) Principal Component Analysis performed on the complete data set of the abundances of 4332 proteins on the 6 biological samples. Individual representation. (B) Volcano plot showing comparative proteomic data between 2Xc1 strain and WTc1 strain at steady state during nitrogen limitation. The red spots indicate proteins selected for being differentially accumulated. On the left side are the down accumulated proteins and on the right side the up-accumulated proteins. (C) Functional classification of the proteome of *T. lutea* and of proteins differentially accumulated between 2Xc1 strain and WTc1. Only proteins with identified functions are reported here.

Fig. 4: Simplified representation of the central metabolism of *T. lutea* and of affected pathways in strain 2Xc1. Up-accumulated proteins are highlighted in red and down-

accumulated ones in blue. The fold changes are indicated in brackets when a difference of accumulation was recorded. Proteins identified in the genome but not in the present proteome are indicated in italics.{Citation}

Table1

Table 1: Carbon partitioning in percentage of carbon in the three nitrogen physiological states. Pt 27, 41 and 117 corresponding to the state of nitrogen limitation, Pt 41 and 74 corresponding to the state of nitrogen repletion and Pt 53, 98 and 119 corresponding to the state of nitrogen depletion(see figure 2). nd is calculated part of carbon that miss for 100% final.

Sample	Nitrogen state	N/C		Storage lipids		Membrane lipids		Carbohydrates		Proteins		Chlorophyll a		nd	
		WTc1	2Xc1	WTc1	2Xc1	WTc1	2Xc1	WTc1	2Xc1	WTc1	2Xc1	WTc1	2Xc1	WTc1	2Xc1
Pt27	limitation	0.09	0.1	3.4	8.4	25.1	23.7	35.2	27.8	39.2	27.3	1.04	0.7	0	12.1
Pt41	repletion	0.13	0.12	2.5	4.8	23.5	26.3	16.2	18.3	45.9	27.2	1.43	0.9	10.5	22.5
Pt53	depletion	0.08	0.09	3.8	8.1	22.7	21.3	33.4	29.7	34.5	22.9	1.07	0.6	4.5	17.4
Pt74	limitation	0.09	0.08	1.9	5.8	21.5	19.9	31.1	34.7	42.2	24.8	0.79	0.7	2.5	14.1
Pt86	repletion	0.14	0.12	1.9	3.7	23	26.3	26.7	14.4	40.2	26.6	1.46	1.3	6.7	27.7
Pt98	depletion	0.09	0.07	0.6	7	21	18.1	30.9	38.9	39.3	24.1	0.87	0.7	7.3	11.2
Pt117	limitation	0.09	0.07	3.2	6.4	27.1	20.7	37.7	42.7	37.7	21.4	0.91	0.5	0	8.3
Pt129	depletion	0.1	0.09	3.9	9.3	26.8	28.4	26.6	28.4	36.2	23.9	1.08	0.9	5.4	9.1
R^2 with N/C				0.06	0.21	0	0.56	0.56	0.96	0.35	0.63	0.78	0.58		

Table2

Table 2. Proteins up-accumulated in 2Xc1 compared to WTc1

Protein ID	Functional classification	Pathways	Protein Name	Synonym	EC	peptides	Log2(fold change)	p-value
P196.01	Central metabolism & energy	Photosynthesis	Cytochrome c6	CyC6		10	1.38	0.00
P3303.01			Cytochrome c6	CyC6		2	5.00	0.00
P31.04			Ferredoxin--NADP reductase	FNR	1.18.1.2	14	1.36	0.02
P1680.01			Ferredoxin	Fd		8	3.26	0.00
P2343.01			PsbP domain containing unknown concerved protein	PsbP		5	1.30	0.01
P235.01			Photosystem II 12 kDa extrinsic protein	PsbU		13	1.83	0.01
P64.01		Calvin cycle & glycolysis / glucogenesis	Phosphoribulokinase	PPK	2.7.1.19	30	1.88	0.00
P9.01			glyceraldehyde-3-phosphate dehydrogenase (NADP+)	GAPDH(NADP+)	1.2.1.13	50	1.37	0.00
P1109.01			Fructose-bisphosphate aldolase	FBPA	4.1.2.13	11	3.57	0.03
P2730.01			Fructose-bisphosphate aldolase	FBPA	4.1.2.13	6	2.01	0.02
P4005.01		Polysaccharides	Callose synthase			3	5.00	0.01
P1607.01		Pyruvate metabolism	Pyruvate dehydrogenase kinase (mitochondrial)	PDHK		10	3.18	0.00
P3289.01		Oxidative phosphorylation	NADH dehydrogenase [ubiquinone] 1 alpha subcomplex assembly factor 5	NADHDH-p5	1.6.5.3	4	1.94	0.00
P748.01		Biosynthesis of sterol compounds	Cycloartenol-C-24-methyltransferase 1			14	2.75	0.04
P2525.01		L-alanine biosynthesis	Cysteine desulfurase	NIFS	2.8.1.7	6	1.53	0.01
P1015.01		Aminoacyl-tRNA biosynthesis	Phenylalanine--tRNA ligase	PheRS	6.1.1.20	11	2.51	0.01
P3826.01		Pyrimidine metabolism	ATP:CMP phosphotransferase	ATCM	2.7.4.14	3	5.00	0.00
P3380.01			Aminomethyltransferase		2.1.2.10	2	5.00	0.00
P1056.01	Catabolism of lipids & carbohydrates	Beta-oxidation	Short-chain 3-hydroxyacyl-CoA dehydrogenase	HCDH	1.1.1.35	11	5.00	0.00
P3630.01	Replication and DNA maintenance	DNA repair	UV excision repair protein	RAD23		2	5.00	0.00
P49.07	Transcription & translation	RNA helicase	Unknown concerved ATP-dependent RNA helicase			1	5.00	0.00
P4096.01		Transcription regulation	Histone deacetylase	HDac	3.5.1.98	2	5.00	0.03
P4013.01			Uncharacterized RNA pseudouridine synthase Mb1738			3	5.00	0.00
P2856.01		Ribosomal proteins	Ribosomal protein L11 methyltransferase	L11 Mtase		4	2.19	0.00
P3113.01			40S ribosomal protein S21-1			3	2.08	0.05
P2012.01			40S ribosomal protein S28 gi			4	2.96	0.01
P2188.01			50S ribosomal protein L28, chloroplastic			5	2.91	0.04
P1378.01			Ribosome biogenesis regulatory protein homolog			11	1.97	0.01
P3863.01		Ribosome biogenesis	Ribosome production factor 1			2	5.00	0.01
P2702.01		tRNA	Aminoacyl tRNA synthase complex-interacting multifunctional protein 1			6	1.98	0.01
P1310.01			5'-3' exoribonuclease			10	1.61	0.00
P2691.01			RNA binding domain containing concerved unknown protein			5	5.00	0.00
P4101.01			C3H			2	5.00	0.00
P3717.01			TFIIF alpha sub-unit			4	5.00	0.02
P2870.01	Pigments, xenobiotic ,vitamins & cofactors metabolism	Biosynthesis of steroids	2-C-methyl-D-erythritol 2,4-cyclodiphosphate synthase	MCS	4.6.1.12	5	3.08	0.01
P348.01		Porphyrin and chlorophyll metabolism	Porphobilinogen synthase	PPBNGS	4.2.1.24	29	1.64	0.00
P143.01			Geranylgeranyl diphosphate reductase			31	2.50	0.00
P3176.01	Catabolism of proteins & amino acids	Amino-acid catabolism	2-oxoisovalerate dehydrogenase subunit alpha	BCKDHA	1.2.4.4	4	5.00	0.00
P775.01		Protease / peptidase	KDEL-tailed cysteine endopeptidase CEP1	AtCP56		15	2.80	0.04
P2807.01			Proline iminopeptidase	PI	3.4.11.5	7	2.42	0.00
P4106.01			Serine carboxypeptidase-like 10	SAT		2	5.00	0.00
P3693.01			Tripeptidyl-peptidase 1	TPP-1		3	5.00	0.00
P1222.01			Carboxyl-terminal-processing protease			13	2.46	0.03
P3417.01			Carboxyl-terminal-processing protease			4	5.00	0.00
P2725.01			Protease Do-like 1, chloroplastic			8	2.72	0.00
P3664.01			Putative tyrosinase-like protein tyr-3			3	5.00	0.00
P1106.01			Unknown concerved signal peptidase			12	1.97	0.00
P3685.01	Signal transduction	Regulation of intracellular calcium	Calcium/calmodulin-dependent protein kinase type II delta chain	CAMPK		3	5.00	0.22
P3333.01			EF-hand calcium-binding domain-containing concerved protein			4	5.00	0.00
P3142.01	Cell cycle, cell division & apoptosis	Cell cycle	Cyclin-dependent kinase C-2	CDK2		4	5.00	0.00
P2261.01		Cycle circadien	Cryptochrome DASH, chloroplastic/mitochondrial			9	2.09	0.05
P3799.01	Post Traductional Modifications	Protein isomerisation	Peptidyl-prolyl cis-trans isomerase FKBP53	PPIase FKBP53	5.2.1.8	3	5.00	0.00
P3486.01			Unknown concerved Peptidylprolyl isomerase			3	5.00	0.01
P3514.01			8 ankyrin repeat domain containing unknown protein			3	2.01	0.00
P1287.01			Hsp70 nucleotide exchange factor FES1			8	1.51	0.00
P840.01			DnaJ homolog subfamily B member 3	DNAJ-B3		19	2.17	0.01
P4113.01	Morphogenesis & motility		ADP-ribosylation factor GTPase-activating protein 1	ARF GAP 1		2	5.00	0.00
P3257.01			Dynein light chain 2, cytoplasmic			4	5.00	0.01

Table3

Table 3. Proteins down-accumulated in 2Xc1

Protein ID	Functional classification	Pathways	Protein name	Synonym	EC	peptides	Log2(fold change)	p-value
P3313.01	Central metabolism & energy	CCM	Carbonic anhydrases	CA	4.2.1.1	2	-1.44	0.00
P1924.01		Photosynthesis	Photosystem I P700 chlorophyll a apoprotein	PsaA		8	-4.00	0.02
P1724.01			Photosystem I P700 chlorophyll a apoprotein A2	PsaB		9	-4.29	0.03
P1833.01		Glycolysis / Gluconeogenesis / Fructose and Mannose metabolism	Phosphoglucomutase	PGCM	5.4.2.2	8	-2.32	0.01
P2352.01			6-phosphofructo-2-kinase/fructose-2, 6-bisphosphatase	PFK-2	2.7.1.105	9	-5.00	0.00
P3407.01			6-phosphofructo-2-kinase/fructose-2, 6-bisphosphatase	PFK-2	2.7.1.105	5	-5.00	0.00
P500.01		Pyruvate & AcCoA metabolism	2-isopropylmalate synthase, chloroplast	IPPSh	2.3.3.13	14	-2.55	0.00
P1538.02			Acetyl-coenzyme A synthetase	ACS	6.2.1.1	4	-5.00	0.01
P183.01			Pyruvate Dehydrogenase Complex E2 (mitochondrial)	PDC-E2	2.3.1.12	19	-2.69	0.01
P1839.01			Acetaldehyde dehydrogenase	ALDH	1.2.1.10	11	-4.6	0.02
P7.01			Pyruvate carboxylase	PCr	6.4.1.1	79	-2.73	0.05
P25.01		TCA & glyoxylate cycles	Aconitate hydratase 2 (Aconitase)	ACO	4.2.1.3	70	-1.98	0.00
P1639.01			Malate synthase G	MALsH	2.3.3.9	13	-5.00	0.00
P78.01			Isocitrate dehydrogenase [NADP]	IDH	1.1.1.42	41	-2.03	0.00
P198.01			2-oxoglutarate dehydrogenase-E1	OGDC-E1	1.2.4.2	31	-4.83	0.01
P3745.01		Oxidative phosphorylation	ATPase		3.6.3.14	4	-5.00	0.00
P246.01			ATP synthase subunit gamma (chloroplastic)	ATPaseG	3.6.3.14	16	-1.97	0.00
P306.01			NADH-dependent fumarate reductase	FR (NADH)	1.3.1.6	30	-1.84	0.00
P306.02			NADH-dependent fumarate reductase	FR (NADH)	1.3.1.6	20	-2.32	0.01
P744.01			NADH dehydrogenase [ubiquinone] flavoprotein	NADHDH-p1	1.6.5.3	15	-3.45	0.00
P4035.01			NADH dehydrogenase	NADHDH-p10	1.6.5.3	3	-5.00	0.01
P3286.01			NADH-quinone oxidoreductase subunit B	NADHOR-p2	1.6.5.3	7	-5.00	0.01
P2511.01		Pentose phosphate pathway	D-Ribulose-5-Phosphate 3-Epimerase	RPEh	5.1.3.1	3	-2.76	0.05
P3320.01			Ribose-phosphate pyrophosphokinase	RPPK	2.7.6.1	5	-5.00	0.00
P1375.01			Transaldolase	TAL	2.2.1.2	9	-3.86	0.01
P1961.01		Mannitol	Mannitol 1-phosphate dehydrogenase	M1PDH	1.1.1.17	9	-4.93	0.01
P173.01		Nitrogen uptake & assimilation	High affinity nitrate transporter 2.5	NRT2		23	-4.19	0.04
P173.02			High affinity nitrate transporter 2.5	NRT2		12	-4.60	0.01
P652.01			Ammonium transporter 1 member 2	AMT1		6	-3.71	0.03
P3974.01		Cyanate decomposition	Cyanate hydratase	Cyanase		3	-5.00	0.00
P191.01		Urea	Urease	Urease	3.5.1.5	36	-2.01	0.00
P1355.01		Amino-acid metabolism	Pyrroline-5-carboxylate reductase		1.5.1.2	9	-2.49	0.00
P2137.01			Cysteine transaminase	CYSTAm	2.6.1.3	7	-2.95	0.04
P2544.01			NAD/NADP-dependent betaine aldehyde dehydrogenase	BADH		7	-1.68	0.00
P2985.01			Glycine C-acetyltransferase		2.3.1.29	4	-5.00	0.00
P780.01			Histidinol-phosphatase, chloroplast	HPh	3.1.3.15	10	-1.27	0.00
P3501.01			Threonine dehydratase	AtSR	4.3.1.19	5	-5.00	0.01
P395.01			Methionine synthase	MatH	2.1.1.13	38	-5.00	0.02
P3539.01			Kynurenine 3-monooxygenase and related flavoprotein monooxygenase			4	-5.00	0.00
P193.01			Aspartate aminotransferase	AST	2.6.1.1	27	-2.66	0.03
P969.01			Phosphoserine aminotransferase	PSAT	2.6.1.52	13	-1.03	0.01
P3849.01			Branched-chain-amino-acid aminotransferase-like protein			2	-5.00	0.00
P3817.01		Aminoacyl-tRNA biosynthesis	Cysteine--tRNA ligase, cytoplasmic	CysRS	6.1.1.16	4	-5.00	0.00
P170.01			Alanine--tRNA ligase	AlaRS	6.1.1.7	39	-3.23	0.02
P341.02			Aspartate--tRNA ligase	AspRS	6.1.1.12	18	-3.08	0.01
P549.01			Cysteine--tRNA ligase	CysRS	6.1.1.16	23	-2.50	0.01
P846.01			Glutamine--tRNA ligase	GlnRS	6.1.1.18	20	-2.39	0.00
P956.01			Probable glutamate--tRNA ligase	GluRS	6.1.1.17	17	-2.45	0.01
P1725.01			Histidine--tRNA ligase	HisRS	6.1.1.21	11	-3.76	0.01
P2809.01			Isoleucine--tRNA ligase	IleRS	6.1.1.5	7	-5.00	0.01
P2276.01			Leucine--tRNA ligase	LeuRS	6.1.1.4	11	-5.00	0.05
P2821.01			Leucine--tRNA ligase	LeuRS	6.1.1.4	6	-4.11	0.01
P609.01			Proline--tRNA ligase	ProRS	6.1.1.15	18	-2.31	0.02
P2501.01			Valine--tRNA ligase	ValRS	6.1.1.9	7	-5.00	0.01
P36.02			Serine--tRNA ligase	SerRS	6.1.1.11	34	-1.99	0.01
P446.01			Threonine--tRNA ligase	THRrs	6.1.1.3	23	-5.00	0.00
P2211.01			Tyrosine--tRNA ligase	TyrRS	6.1.1.1	9	-5.00	0.02
P960.01		Pyrimidine metabolism	thioredoxin-disulfide reductase, cytosol	TDSR	1.8.1.9	14	-2.23	0.01
P3196.01		Purine metabolism	Bifunctional purine biosynthesis protein		3.4.24	5	-5.00	0.00
P2028.01			nucleoside-triphosphate phosphatase			9	-3.31	0.02

P335.02			Glycolipid transfer protein	GLTP		9	-2.15	0.00
P2580.01		Carbohydrate catabolism	Lysosomal beta glucosidase	GH3	3.2.1.21	9	-5.00	0.00
P3802.01			Mannosyl-oligosaccharide glucosidase GCS1	GH63	3.2.1.106	4	-5.00	0.02
P2632.01			Lysophosphatidic acid-acyltransferase	LPAT	2.3.1.51	8	-5.00	0.00
P1115.01		Very long chain Fatty acid biosynthesis	Very-long-chain 3-oxoacyl-CoA reductase 1	Kcr	1.1.1.330	11	-2.22	0.02
P815.01		Glycerophospholipid metabolism	Phosphatidylglycerophosphatase		3.1.3.27	8	-1.42	0.01
P514.01		Isoprenoid metabolism	Methylcrotonoyl-CoA carboxylase subunit alpha	Mccase	6.4.1.4	23	-4.53	0.01
P351.01		Beta-oxidation	Long chain acyl-CoA synthetase	LACS	6.2.1.3	21	-2.80	0.01
P3689.01	Lipids & carbohydrates		Long chain acyl-CoA synthetase	LACS	6.2.1.3	3	-5.00	0.00
P518.02			Long chain acyl-CoA synthetase	LACS	6.2.1.3	4	-3.91	0.02
P2895.01			3-ketoacyl-CoA thiolase	ACAA	2.3.1.16	7	-5.00	0.02
P59.01			Long chain 3-hydroxyacyl-CoA dehydrogenase	HCDH	1.1.1.35	39	-1.37	0.00
P621.01			3-hydroxyacyl-CoA dehydrogenase	HCDH	1.1.1.35	20	-3.05	0.01
P23.01		Membrane lipid metabolism	Glycerol-3-phosphate dehydrogenase (NAD+)	G3PDH(NAD+)	1.1.1.8	32	-1.23	0.01
P383.01			Glycerol-3-phosphate dehydrogenase	G3PDH-M	1.1.1.8	24	-2.47	0.01
P1738.01			Lysophospholipase	LPL		6	-3.11	0.05
P4043.01		Triacylglycerol catabolism	Triacylglycerol hydrolase	TAGH	3.1.1.3	2	-5.00	0.18
P380.01			3-isopropylmalate dehydratase, 3-Carboxy-2-hydroxy-4-methylpentanoate forming		4.2.1.33	24	-2.70	0.01
P2762.01		Amino-Acid catabolism	Unknown concerved glutaminase			5	-5.00	0.00
P24.01			Periplasmic L-aminoacid oxydase	PLAAOX		56	-2.22	0.05
P3880.01			3-hydroxyanthranilate 3,4-dioxygenase	3HOA	1.13.11.6	4	-5.00	0.00
P2841.01		Protease / peptidase	Probable Xaa-Pro aminopeptidase P	AMPP		3	-2.62	0.00
P3629.01			Probable Xaa-Pro aminopeptidase P	AMPP		3	-5.00	0.00
P476.01			Presequence protease 1	AtPreP1		30	-3.35	0.04
P2736.01			26S proteasome non-ATPase regulatory subunit 1 homolog B	AtRPN2b		9	-5.00	0.04
P713.01			Ubiquitin carboxyl-terminal hydrolase 12	AtUBP12		27	-3.92	0.02
P588.01			Ubiquitin carboxyl-terminal hydrolase 7	AtUBP7		16	-2.40	0.00
P912.01			Proteasome subunit beta type-6	DAPS-1		14	-2.35	0.01
P3296.01			Glutamate carboxypeptidase 2	FGCP		4	-5.00	0.00
P268.01	Catabolism of proteins & amino acids		Puromycin-sensitive aminopeptidase	PSA		37	-2.92	0.02
P3967.01			E3 ubiquitin-protein ligase UPL3			3	-5.00	0.01
P1878.01			ATP-dependent protease subunit HslV			6	-3.15	0.01
P3704.01			Presequence protease			4	-5.00	0.00
P1819.01			Probable aminopeptidase NPEPL1			8	-1.52	0.01
P776.01			Probable cytosolic oligopeptidase A			21	-2.09	0.00
P3924.01			Protease 2			2	-5.00	0.00
P820.01			Ubiquitin carboxyl-terminal hydrolase 5			21	-2.78	0.00
P2831.01			Ubiquitin-like modifier-activating enzyme 1			5	-2.43	0.04
P541.01			Uncharacterized peptidase y4nA			21	-2.06	0.02
P3901.01			Unknown concerved peptidase			3	-5.00	0.00
P187.01		ND	Methylmalonyl-CoA mutase	mcm	5.4.99.2	26	-2.54	0.00
P693.01		Chaperones and HSP	T-complex protein 1 subunit alpha	TCP-1-alpha		21	-3.11	0.03
P263.01			T-complex protein 1 subunit gamma	TCP-1-gamma		28	-2.12	0.05
P18.01			ATP-dependent Clp protease ATP-binding subunit clpA	ClpC		56	-2.07	0.03
P108.01			HSP_90			51	-1.23	0.01
P3961.01			Heat shock protein sti1 homolog	HSP		3	-5.00	0.01
P100.01			Heat shock Protein 70	HSP70		45	-4.71	0.01
P17.01			Heat shock protein 90-1	HSP90		62	-2.07	0.02
P18.02			Chaperone protein ClpB	ClpB		25	-2.43	0.03
P18.04			Chaperone protein ClpC1, chloroplastic			17	-4.03	0.01
P3552.01		Phosphorylation	Glucuronokinase 1	AtGlcAK1		6	-5.00	0.04
P4033.01			Probable protein phosphatase 2C 48	OsPP2C48		2	-5.00	0.00
P2745.01			Unknown phosphatase			5	-5.00	0.01
P3904.01	Post translational modifications		Protein phosphatase 1 regulatory subunit pprA			3	-5.00	0.00
P2312.01			Serine/threonine-protein phosphatase 4 regulatory subunit			9	-5.00	0.00
P1341.01			Serine/threonine-protein phosphatase 4 regulatory subunit 1			8	-1.46	0.01
P2078.01		Glycosylation	UDP-glucose:glycoprotein glucosyltransferase			15	-5.00	0.05
P1316.01		Isomerization	Protein disulfide-isomerase 5-3	AtPDIL5-3		14	-2.94	0.00
P2457.01			Peptidyl-prolyl cis-trans isomerase B	PPIase B	5.2.1.8	6	-1.39	0.01
P4138.01			Peptidyl-prolyl cis-trans isomerase CYP18-4	PPIase CYP18-4	5.2.1.8	1	-5.00	0.00
P3888.01			Peptidyl-prolyl cis-trans isomerase cyp3	PPIase cyp3	5.2.1.8	2	-5.00	0.00
P862.01			Peptidyl-prolyl cis-trans isomerase FKBP62	PPIase FKBP62	5.2.1.8	15	-1.92	0.00
P3749.01			Peptidyl-prolyl cis-trans isomerase FKBP65	PPIase FKBP65	5.2.1.8	5	-5.00	0.01
P386.01		Ubiquitination	U-box domain-containing protein 12	OsPUB12		23	-1.28	0.00
P4022.01			SUMO-activating enzyme subunit 2			2	-5.00	0.00
P3596.01			Peptide methionine sulfoxide reductase	MSRA		3	-5.00	0.00

P3784.01			Alpha N-terminal protein methyltransferase 1			2	-5.00	0.00
P1851.01		Oxidative stress response	Glutathione S-transferase theta-2	GST		7	-2.14	0.04
P2339.01			Thioredoxin domain-containing protein 5	ER protein 46		4	-1.17	0.00
P977.01			Thioredoxin	Trx		8	-1.14	0.00
P1715.01			Thioredoxin-like protein slr0233			8	-1.35	0.01
P3797.01			Lon Protease			3	-5.00	0.00
P3526.01		Chromosome structure	Structural maintenance of chromosomes protein 1	SMC 1		6	-5.00	0.01
P3485.01			Structural maintenance of chromosomes protein 3	SMC 3		5	-5.00	0.00
P2789.01			Structural maintenance of chromosomes protein 5	SMC 5		7	-5.00	0.00
P1802.01		Replication	DNA topoisomerase 2	DNA topo-2	5.99.1.3	8	-3.76	0.00
P3972.01			DNA replication licensing factor mcm2	MCM2		2	-5.00	0.01
P3931.01			DNA replication licensing factor mcm4	MCM4		2	-5.00	0.00
P3174.01			DNA replication licensing factor MCM5	MCM5		7	-5.00	0.00
P4028.01			DNA replication licensing factor mcm6	MCM6		2	-5.00	0.01
P3646.01	Replication & DNA maintenance		Replication factor C subunit 3	RFC-3	3.6.1.15	3	-5.00	0.00
P2418.01			Replication factor C subunit 5	RFC-5	3.6.1.15	6	-2.24	0.00
P2713.01			Replication protein A 70 kDa DNA-binding subunit	RPA1		5	-2.75	0.02
P3709.01			Replication protein A 70 kDa DNA-binding subunit C	RPA1		3	-5.00	0.00
P3299.01			Mitochondrial DNA replication protein YHM2	YHM2		4	-5.00	0.00
		DNA reparation	Double-strand-break repair protein rad21	RAD21		2	5.00	0.00
P3279.01		ND	Polyribonucleotide nucleotidyltransferase	PNPase		6	-5.00	0.01
P33.01			14-3-3-like protein F			47	-1.03	0.01
P805.01			Putative chromatin-remodeling complex ATPase chain			16	-3.17	0.01
P2287.01		RNA helicase	ATP-dependent RNA helicase dbp9			5	-2.38	0.02
P1784.01			DEAD-box ATP-dependent RNA helicase 21			8	-2.22	0.04
P4124.01			DEAD-box ATP-dependent RNA helicase 52B			2	-5.00	0.01
P3574.01			Unknown concerved ATP-dependent RNA helicase			3	-5.00	0.00
P3443.01		RNA polymerases	DNA-directed RNA polymerase II subunit rpb1	RNA pol		7	-5.00	0.00
P4131.01			DNA-directed RNA polymerases I, II, and III subunit RPABC1	RNA pol		2	-5.00	0.01
P3804.01			Non-canonical poly(A) RNA polymerase PAPD7	TUTase 5		4	-5.00	0.00
P441.01			Mediator of RNA polymerase II transcription subunit 36a			16	-1.29	0.00
P1273.01		RNA-binding protein	SRP72 RNA-binding domain containing unknown protein			11	-3.94	0.00
P3062.01		Splicing	Pre-mRNA-splicing factor			5	-5.00	0.01
P2007.01		Transcription factors	HB-other			7	-3.15	0.00
P3527.01			HB-other			4	-5.00	0.00
P1797.01			MYB (2R)			9	-2.08	0.01
P420.01		Elongation	Elongation factor 3	EF-3		21	-3.21	0.03
P773.01			Elongation factor P	EF-P		12	-1.22	0.00
P2355.01			Elongation factor G	EfG		12	-5.00	0.01
P1185.01		initiation factor	Eukaryotic translation initiation factor 2D	eIF2d		12	-2.19	0.01
P3325.01			Eukaryotic translation initiation factor 3 subunit A	eIF3a		3	-5.00	0.02
P888.01	Transcription & translation		Eukaryotic translation initiation factor 3 subunit B	eIF3b		14	-2.84	0.02
P3469.01			Probable translation initiation factor eIF-2B subunit epsilon			3	-5.00	0.01
P701.01			Translation initiation factor IF-2			22	-2.80	0.04
P4009.01		Ribosomal proteins	30S ribosomal protein S1 homolog A			2	-5.00	0.01
P3890.01			4 ankyrin repeat domain containing unknown protein			3	-5.00	0.00
P188.01			40S ribosomal protein S3-3			12	-2.15	0.03
P3936.01			5'-3' exoribonuclease			2	-5.00	0.00
P3746.01			3-hydroxyisobutyryl-CoA hydrolase		3.1.2.4	2	-5.00	0.00
P3499.01			6 ankyrin repeat domain containing Serine/threonine-protein phosphatase			3	-5.00	0.00
P2411.01			60S ribosomal protein L15-1			2	-2.49	0.05
P292.01			60S ribosomal protein L9			15	-2.59	0.03
P2340.01		Transcription	CCR4-NOT transcription complex subunit 8	CALIFp		6	-2.18	0.01
P811.01			Pre-mRNA-processing factor 6			16	-4.25	0.03
P3625.01			CCR4-NOT transcription complex subunit 1			4	-5.00	0.19
P4108.01			CCR4-NOT transcription complex subunit 11			2	-5.00	0.19
P1732.01			CCR4-NOT transcription complex subunit 3			9	-1.86	0.05
P2668.01			m7GpppX diphosphatase		3.6.1.59	7	-2.15	0.02
P1897.01			Transcription elongation factor SPT6			10	-3.84	0.02
P3487.01			Unknown NAD+ ADP-ribosyltransferase			4	-5.00	0.02
P1800.01			1-deoxy-D-xylulose-5-phosphate synthase	DXS	2.2.1.7	9	-4.05	0.01
P1228.01			6-thioxanthine 5'-monophosphate:L-glutamine amido-ligase		6.3.5.2	12	-3.58	0.01
P1114.01	Pigments, xenobiotic ,vitamins &		Inositol hexakisphosphate and diphosphoinositol-pentakisphosphate kinase 1			16	-4.65	0.05
P110.01	cofactors metabolism		Fucoxanthin-chlorophyll a-c binding protein E			11	-1.81	0.01
P175.01			Fucoxanthin-chlorophyll a-c binding protein E			23	-1.40	0.00
P2310.01			Cyanuric acid amidohydrolase		3.5.2.15	8	-3.51	0.00

P4099.01			Purple acid phosphatase 21			2	-5.00	0.00
P2930.01			Calcium/calmodulin-dependent protein kinase type II delta chain	CAMPK		8	-5.00	0.03
P1830.01			Calcium/calmodulin-dependent protein kinase type 1	CAMPK		8	-1.06	0.00
P305.01		Regulation of intracellular calcium	Calcium/calmodulin-dependent protein kinase type 1D	CAMPK		19	-2.34	0.00
P2539.01			EF-hand calcium-binding domain-containing concerved protein			8	-2.04	0.00
P3233.01			EF-hand calcium-binding domain-containing concerved protein			4	-5.00	0.00
P1366.01			EF-hand domain-containing family member C2			11	-3.40	0.03
P3307.01	Signal transduction		Phototropin			4	-5.00	0.00
P305.02			Extracellular signal-regulated kinase 2	ERK2		8	-2.79	0.00
P1163.01			Glycogen synthase kinase-3 beta	GSK-3 beta		5	-2.94	0.00
P3480.01			Signal recognition particle receptor subunit alpha	SR-alpha		2	-2.21	0.04
P1279.01			TNF receptor-associated protein 1 homolog, mitochondrial			13	-3.13	0.01
P1942.01			Mitochondrial import receptor subunit TOM40-1	TOM40		7	-3.52	0.00
P2928.01			Mitochondrial import receptor subunit tom70	TOM70		6	-5.00	0.00
P2151.01			COP9 signalosome complex subunit 4	AtS4		12	-5.00	0.04
P1437.01			Signal recognition particle subunit SRP68	SRP68		11	-2.96	0.00
P3203.01			Serine/threonine-protein phosphatase 2A 65 kDa regulatory subunit A	PP2RA		8	-5.00	0.01
P3530.01			Cytoskeleton-associated AAA family ATPase			4	-5.00	0.00
P2822.02			Interferon-induced guanylate-binding protein			4	-5.00	0.00
P2690.01			Microtubule-associated protein			5	-2.69	0.00
P2787.01			Myosin			7	-5.00	0.00
P2115.01			Myosin and Kinesin motor domain containing unknown protein			6	-2.35	0.00
P1242.01			Myosin-6			20	-3.80	0.00
P1808.01	Morphogenesis & motility		Parafibromin			5	-1.61	0.01
P3433.01			Vesicle-fusing ATPase			5	-5.00	0.00
P1376.01			Cortactin-binding protein 2	CortBP2		8	-2.53	0.00
P3772.01			Dynactin subunit 1	DP-150		2	-5.00	0.01
P117.01			ADP-ribosylation factor 1			13	-2.06	0.03
P1614.01			ADP-ribosylation factor 1			7	-3.48	0.03
P124.01			Alpha-actinin A			46	-2.44	0.04
P2672.01			Flagellar protein			8	-5.00	0.03
P276.01			V-type proton ATPase subunit A	V-ATPase	3.6.3.14	22	-2.87	0.05
P3519.01			Coatomer subunit alpha-2	Alpha-COP 2		5	-5.00	0.01
P142.01			ADP,ATP carrier protein	ANT		18	-3.03	0.03
P1037.01			Coatomer subunit epsilon-1	Epsilon-COP 1		9	-2.41	0.03
P3447.01			Transportin-1	MIP		4	-2.64	0.02
P3030.01			Vacuolar iron transporter 1.2	OsVIT1.2		2	-3.15	0.03
P3490.01			Vesicle transport v-SNARE protein	V-SNARE		4	-5.00	0.00
P2670.01	Transport & Secretion		ABC transporter B			7	-5.00	0.01
P3813.01			ADP-ribosylation factor			2	-5.00	0.00
P3819.01			ADP-ribosylation factor			3	-5.00	0.00
P3054.01			Calcium-transporting ATPase 1, endoplasmic reticulum-type			5	-5.00	0.05
P2466.01			Translocation protein SEC63 homolog			8	-5.00	0.00
P3175.01			Vacuolar protein sorting-associated protein 52 A			6	-5.00	0.00
P2285.01			Vacuolar protein sorting-associated protein 45			8	-2.63	0.01
P3995.01			AP-1 complex subunit mu			2	-5.00	0.02

Figure1

Click here to download high resolution image

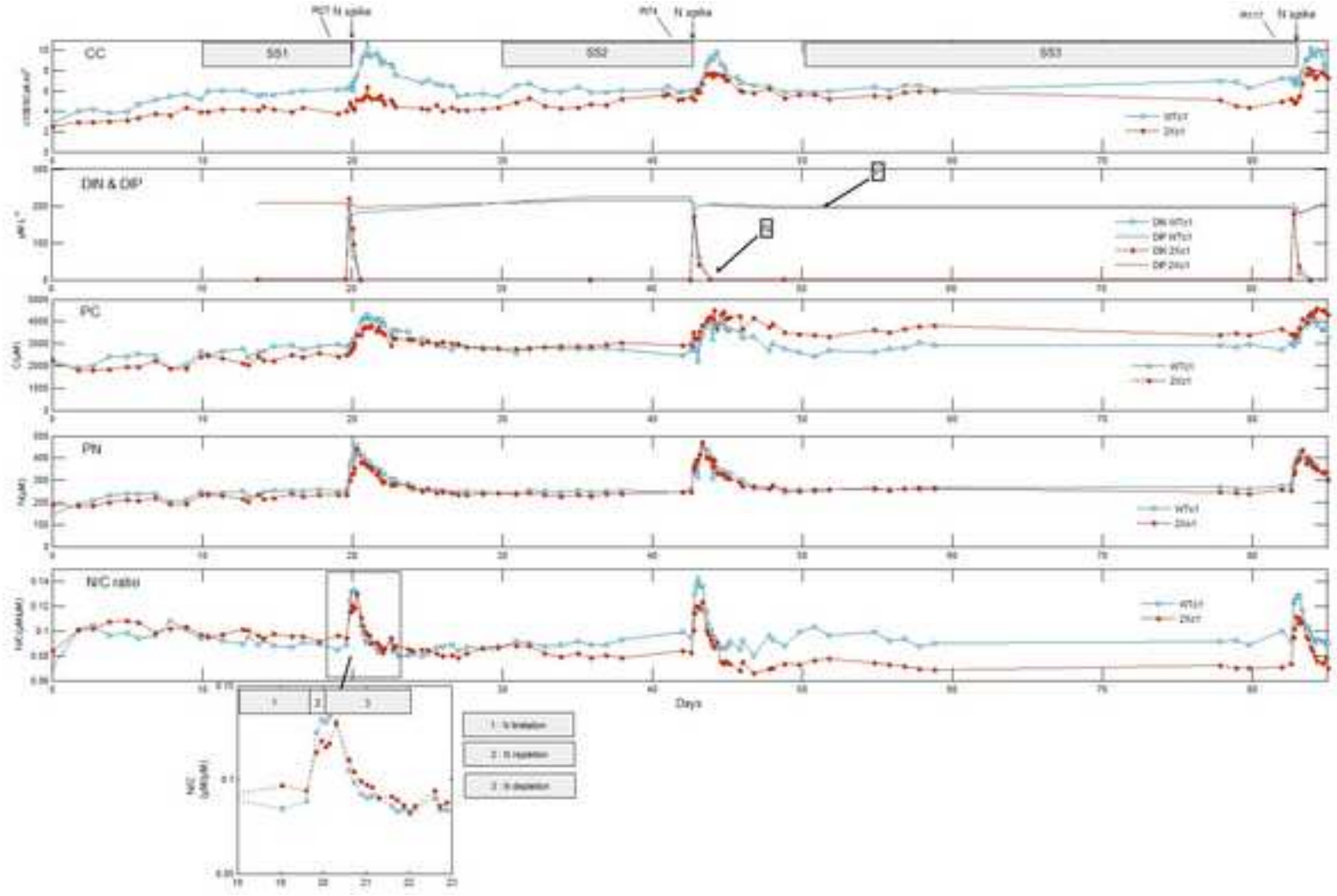

Figure2

Click here to download high resolution image

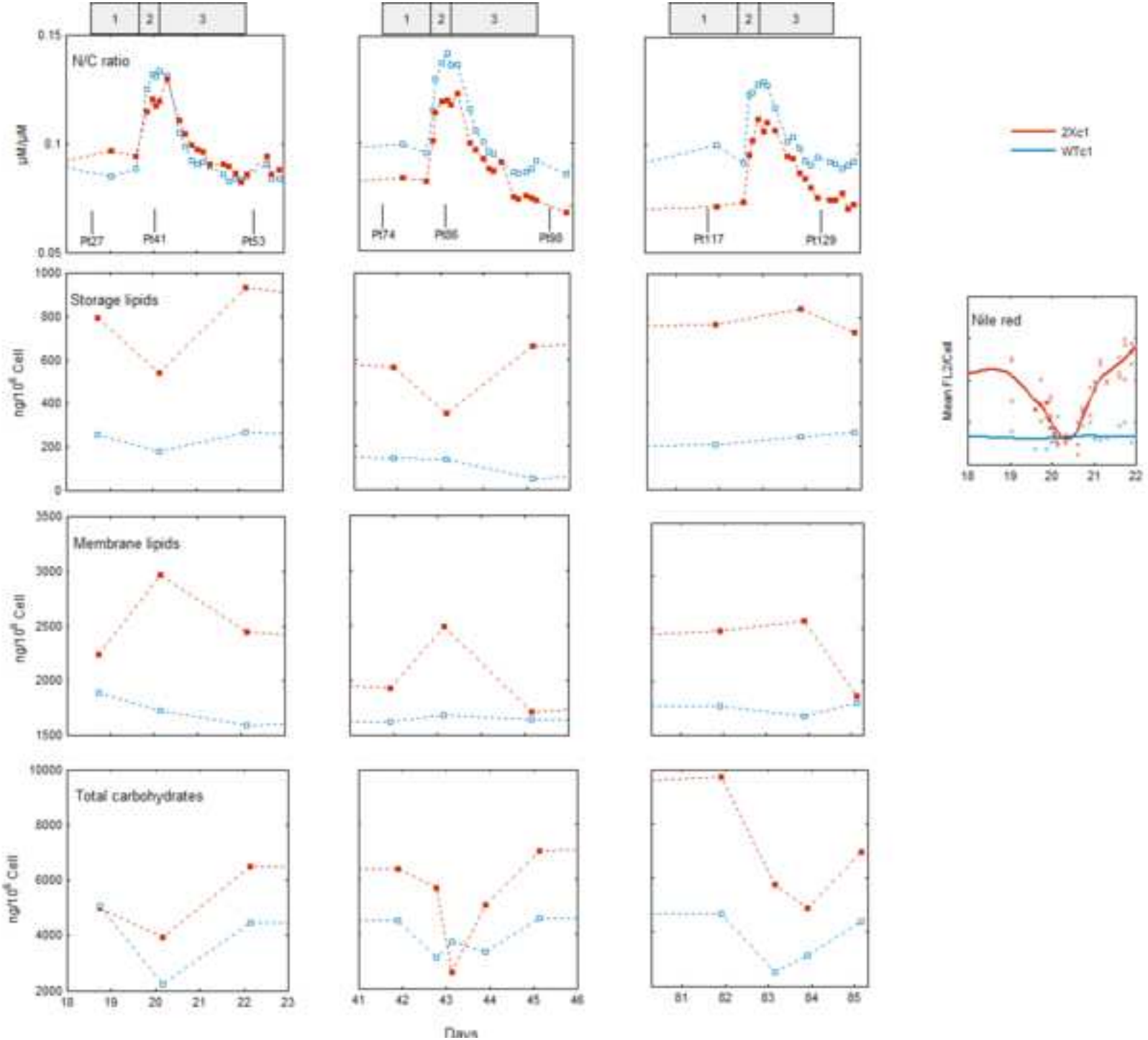

Figure3

Click here to download high resolution image

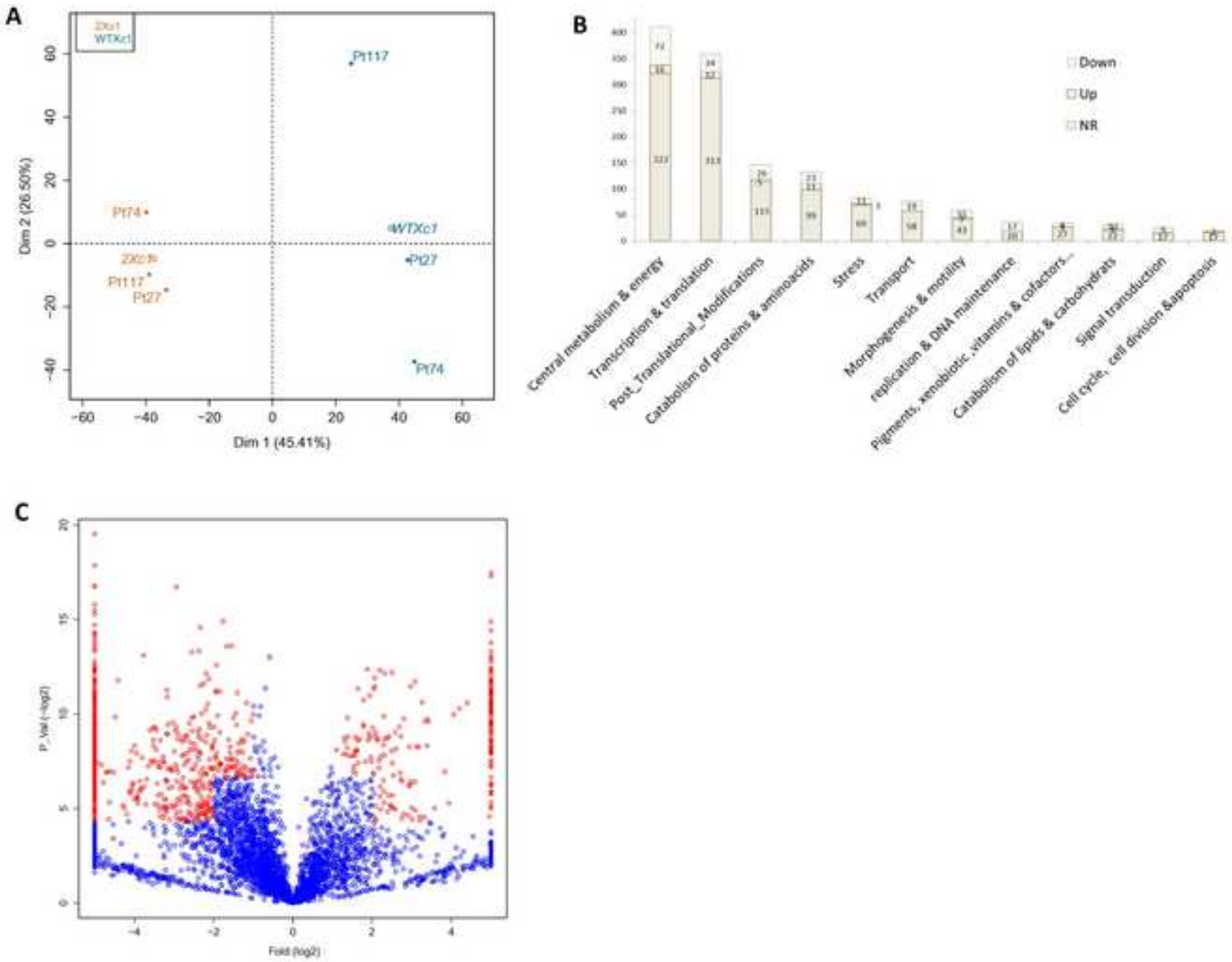

Figure4

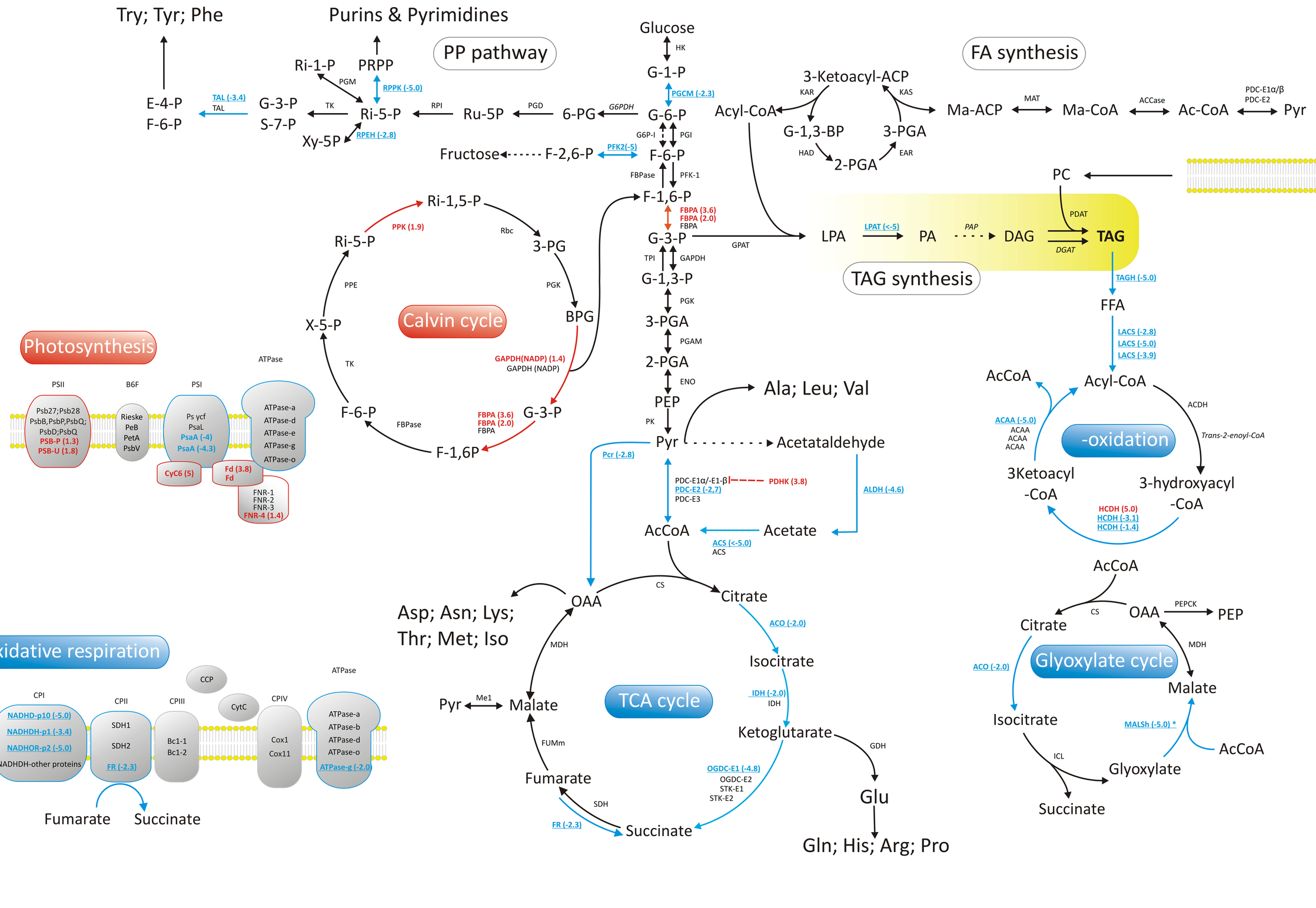
Try; Tyr; Phe
Purins & Pyrimidines
PP pathway
FA synthesis
Glucose
HK
G-1-P
PGCM (-2.3)
G-6-P
G6P-I
PGI
F-6-P
PFK2(-5)
Fructose
F-2,6-P
FBPase
PFK-1
F-1,6-P
FBPA (3.6)
FBPA (2.0)
FBPA
G-3-P
TPI
GAPDH
G-1,3-P
PGK
3-PGA
PGAM
2-PGA
ENO
PEP
PK
Pyr
Acetataldehyde
ALDH (-4.6)
Acetate
ACS (<-5.0)
ACS
AcCoA
Pcr (-2.8)
PDC-E1α/-E1-β
PDC-E2 (-2,7)
PDC-E3
PDHK (3.8)
Ala; Leu; Val
E-4-P
F-6-P
TAL (-3.4)
TAL
G-3-P
S-7-P
TK
Ri-5-P
RPI
Ru-5P
PGD
6-PG
G6PDH
Ri-1-P
PRPP
PGM
RPPK (-5.0)
Xy-5P
RPEH (-2.8)
Ri-1,5-P
Rbc
3-PG
PPK (1.9)
Ri-5-P
PPE
X-5-P
TK
F-6-P
FBPase
F-1,6P
Calvin cycle
BPG
PGK
GAPDH(NADP) (1.4)
GAPDH (NADP)
G-3-P
FBPA (3.6)
FBPA (2.0)
FBPA
3-Ketoacyl-ACP
KAR
KAS
Acyl-CoA
G-1,3-BP
3-PGA
HAD
EAR
2-PGA
Ma-ACP
MAT
Ma-CoA
ACCase
Ac-CoA
PDC-E1α/β
PDC-E2
Pyr
PC
PDAT
LPA
LPAT (<-5)
PA
PAP
DAG
DGAT
TAG
TAG synthesis
TAGH (-5.0)
FFA
LACS (-2.8)
LACS (-5.0)
LACS (-3.9)
AcCoA
Acyl-CoA
ACDH
Trans-2-enoyl-CoA
-oxidation
ACAA (-5.0)
ACAA
ACAA
ACAA
3Ketoacyl
-CoA
3-hydroxyacyl
-CoA
HCDH (5.0)
HCDH (-3.1)
HCDH (-1.4)
Photosynthesis
PSII
B6F
PSI
ATPase
Psb27;Psb28
PsbB,PsbP,PsbQ;
PsbD;PsbQ
PSB-P (1.3)
PSB-U (1.8)
Rieske
PeB
PetA
PsbV
Ps ycf
PsaL
PsaA (-4)
PsaA (-4.3)
ATPase-a
ATPase-d
ATPase-e
ATPase-g
ATPase-o
CyC6 (5)
Fd (3.8)
Fd
FNR-1
FNR-2
FNR-3
FNR-4 (1.4)
Oxidative respiration
CPI
CPII
CPIII
CCP
CytC
CPIV
ATPase
NADHD-p10 (-5.0)
NADHDH-p1 (-3.4)
NADHOR-p2 (-5.0)
NADHDH-other proteins
SDH1
SDH2
FR (-2.3)
Bc1-1
Bc1-2
Cox1
Cox11
ATPase-a
ATPase-b
ATPase-d
ATPase-o
ATPase-g (-2.0)
Fumarate
Succinate
Asp; Asn; Lys;
Thr; Met; Iso
OAA
CS
Citrate
ACO (-2.0)
Isocitrate
IDH (-2.0)
IDH
Ketoglutarate
GDH
Glu
Gln; His; Arg; Pro
TCA cycle
MDH
Pyr
Me1
Malate
FUMm
Fumarate
SDH
FR (-2.3)
Succinate
OGDC-E1 (-4.8)
OGDC-E2
STK-E1
STK-E2
AcCoA
CS
OAA
PEPCK
PEP
Citrate
ACO (-2.0)
Glyoxylate cycle
MDH
Malate
Isocitrate
MALSh (-5.0) *
AcCoA
ICL
Glyoxylate
Succinate